



Spatiotemporal denudation rates of the Swabian Alb escarpment (southwestern Germany) dominated by anthropogenic impact, lithology, and base-level lowering

Mirjam Schaller^{1,2}, Daniel Peifer¹, Alexander B. Neely¹, Thomas Bernard¹, Christoph Glotzbach¹,
Alexander R. Beer¹, and Todd A. Ehlers²

¹Department of Geosciences, University of Tuebingen, 72076 Tuebingen, Germany

²School of Geographical and Earth Sciences, University of Glasgow, Glasgow, UK

Correspondence: Mirjam Schaller (mirjam.schaller@glasgow.ac.uk)

Received: 30 August 2024 – Discussion started: 20 September 2024

Revised: 8 April 2025 – Accepted: 21 April 2025 – Published: 21 July 2025

Abstract. Surface denudation rates, a composite of physical erosion and chemical weathering, are governed by the tectonic, lithologic, climatic, and biotic conditions of a landscape and anthropogenic disturbances. Quantifying rates and disentangling their causes is challenging but important for understanding and predicting landscape evolution over space and time. In this study, we focus on a low-relief and mixed-lithology mountain range (Swabian Alb, southwestern Germany), whose 200–400 m high escarpment and foreland drain to the Neckar River to the north and whose plateau drains into the Danube River to the southeast. These two drainage systems are subjected to similar uplift rates and climate and biotic conditions but contain different lithologies, base levels, and topography. We calculate decadal-timescale chemical weathering and physical erosion rates based on 43 locations with suspended and dissolved river load measurements and compare them to published longer-term rates (e.g., denudation, incision, uplift).

Chemical weathering rates (based on the dissolved river load and discharge and corrected for atmospheric and anthropogenic input) range from 0.003–0.070 mm yr⁻¹, while physical erosion rates (calculated from suspended river load and discharge) range from 0.001–0.072 mm yr⁻¹. The catchment-wide denudation rates range from 0.005–0.119 mm yr⁻¹, resulting in ratios of chemical weathering over total denudation rate (W/D) between 0.40 and 0.99. These high values indicate that chemical weathering is generally the dominant denudation process in this cool to temperate humid setting dominated by sedimentary rocks. Both physical erosion and chemical weathering rates are higher in tributaries draining towards the north/Neckar River than in rivers draining towards the southeast/Danube River, resulting in southeastern escarpment retreat rates of 1.0–8.1 mm yr⁻¹. The anthropogenic effects on denudation rates were evaluated using the Human Footprint and Connectivity Status indices (HFI and CSI, respectively) and the area of artificial constructions for each catchment. After a simplified correction for either index, the natural (non-anthropogenic) denudation rates are estimated to be lower than the values reported above, although it is unclear how to accurately correct rates with either index. Regardless of how the correction of anthropogenic impact is applied, we find denudation rates are consistently higher for the Neckar Swabian Alb tributaries.

Comparison of W/D values from the Swabian Alb to other study areas in different tectonic, lithologic, and climatic settings with W/D values ranging from 0.1–1.0 suggests the W/D values in the Swabian Alb (> 0.4) result from high and lithology-dependent chemical weathering rates. The high W/D ratio likely results from late Cenozoic base-level lowering of the Neckar River that resulted in south-to-southeast-directed escarpment retreat across southwestern Germany. Differences in chemical weathering and physical erosion rates across the escarpment divide may arise from either the contrast in topographic relief or the exposure of lithologies in the Neckar catchment that are more susceptible to chemical weathering and physical erosion.

1 Introduction

Landscape denudation rates are influenced by tectonics, lithology, climate, biota, and anthropogenic land use. Denudation is the composite of physical erosion and chemical weathering by biotic and abiotic processes (e.g., Dietrich and Perron, 2006; Schaller and Ehlers, 2022). Disentangling and quantifying spatial and temporal variations in weathering and erosion from biotic and abiotic processes is challenging due to poorly understood interactions between these processes and limitations in the measurement techniques used. However, rates integrating over different timescales can be used to address a broad suite of connections among denudation, short-term anthropogenic impact and land use, and long-term geological processes including active tectonics and ecosystem dynamics (e.g., Hewawasam et al., 2003; Vanacker et al., 2007; Kirby and Whipple, 2012; Sharma and Ehlers, 2023; Ehlers et al., 2022). They can also be used to improve our understanding of the geologic CO₂ budget and its influence on global climate (e.g., Raymo et al., 1988; Maher and Chamberlain, 2014; Bufo et al., 2024). Here we evaluate the physical erosion and chemical weathering rates for two large catchments (the Neckar and Danube rivers) in southwestern Germany that have different base levels and form a continental divide across the Swabian Alb escarpment. In doing this, we investigate how differences in lithology, topography, and base level between these catchments contribute to differences in chemical weathering and physical erosion rates.

Previous studies have laid the groundwork for understanding how the mass balance of landscapes and different measurements can be used to quantify chemical weathering, physical erosion, and total denudation rates (e.g., Gaillardet et al., 1999; Riebe et al., 2003; von Blanckenburg et al., 2012). In the following, a conceptual overview is presented for the relevant processes (Fig. 1a) and governing equations considered in this study (Fig. 1b). Measurements available for quantifying the mass balance are sensitive to processes recorded over different timescales. There is currently no accepted procedure to bridge across the different timescales used by methods presented here, but we highlight their individual sensitivities, as they are implicit in the approaches presented. For example, over decadal timescales (Fig. 1, left side), catchment-wide denudation rates (D) are often determined by making use of catchment area (A), river discharge (Q_w), and total suspended and dissolved solids (TSSs and TDSs, respectively). Measurement of the previous quantities allows determination of the physical erosion rates (E) and chemical weathering rates (W ; e.g., Gaillardet et al., 1999; Meybeck, 1986). The denudation rates based on river load include (amongst other things) deep weathering of bedrock and saprolite but are problematic for capturing bedload transport and sediment transport during infrequent but large-magnitude events (e.g., Turowski et al., 2010). Over

millennial timescales (Fig. 1, right side), catchment-wide denudation rates (D) for quartz-bearing lithologies can be determined with (for example) in situ-produced cosmogenic ¹⁰Be in river sand (e.g., Brown et al., 1995; Granger et al., 1996). Combining these rates with measurements from immobile elements (e.g., Zr) in soil and unweathered bedrock allows the partitioning into E and W (Riebe et al., 2003). Calculation of the ratio of chemical weathering rates over total denudation rate (W/D) provides a simple metric for understanding the relative strengths of chemical vs. physical processes active (e.g., Riebe et al., 2004; West et al., 2005; Ott et al., 2023). For example, W/D values range from 0–1 and reflect total denudation governed by physical erosion, E ($W/D = 0$), or chemical weathering, W ($W/D = 1$). Deep weathering in landscapes over millennial timescales (Fig. 1, right side) is quantifiable by measurement of immobile elements collected from Zr concentrations measured in soil, saprolite, and unweathered bedrock (e.g., Dixon et al., 2009; Riebe and Granger, 2013; Regard et al., 2016). However, the time-intensive quantification of weathering rates with immobile elements is often replaced by measuring TDSs (anions, cations) and Q_w (Fig. 1, left side; e.g., Campbell et al., 2022).

Recent work attempting to understand catchment-wide D has been expanded not only from ¹⁰Be to in situ-produced ³⁶Cl in carbonates but also to incorporate the effect of deep weathering with TDSs (e.g., Ryb et al., 2014). It has also been shown that the coupling of in situ-produced ¹⁰Be in quartz and ³⁶Cl in carbonates from river sand allows the determination of both E and W (e.g., Ott et al., 2022, 2024). In addition, E and W of basaltic, silicate, and carbonate lithologies are more often determined with the technique of meteoric ¹⁰Be (e.g., von Blanckenburg et al., 2012; Wittmann et al., 2015, 2024; Dannhaus et al., 2018). Such D values have also been compared to rates derived from in situ-produced ¹⁰Be in rivers draining silicate lithologies (e.g., VanLandingham et al., 2022).

One of the common challenges, also relevant to this study, is the quantification of the spatial and temporal variability in W , E , and D recorded by different approaches (e.g., left vs. right side of Fig. 1). For example, rates based on river-dissolved solids (over decadal timescales) and in situ-produced cosmogenic nuclides (over millennial timescales) encompass vastly different timescales. Rates derived from in situ-produced cosmogenic ¹⁰Be may integrate processes active from the Last Glacial Maximum to the present, whereas rates based on river load span only the duration of time over which the measurements are recorded (e.g., 10 s to ~ 100 years). In contrast, the method outlined by Riebe et al. (2003) reports both W and E over thousands of years. However, this method may be limited by the spatial distribution of lithologies (e.g., Burke et al., 2007; Heimsath and Burke, 2013) and denudation hotspots (e.g., Larsen et al., 2014). Hence, each method and, more importantly, the combination

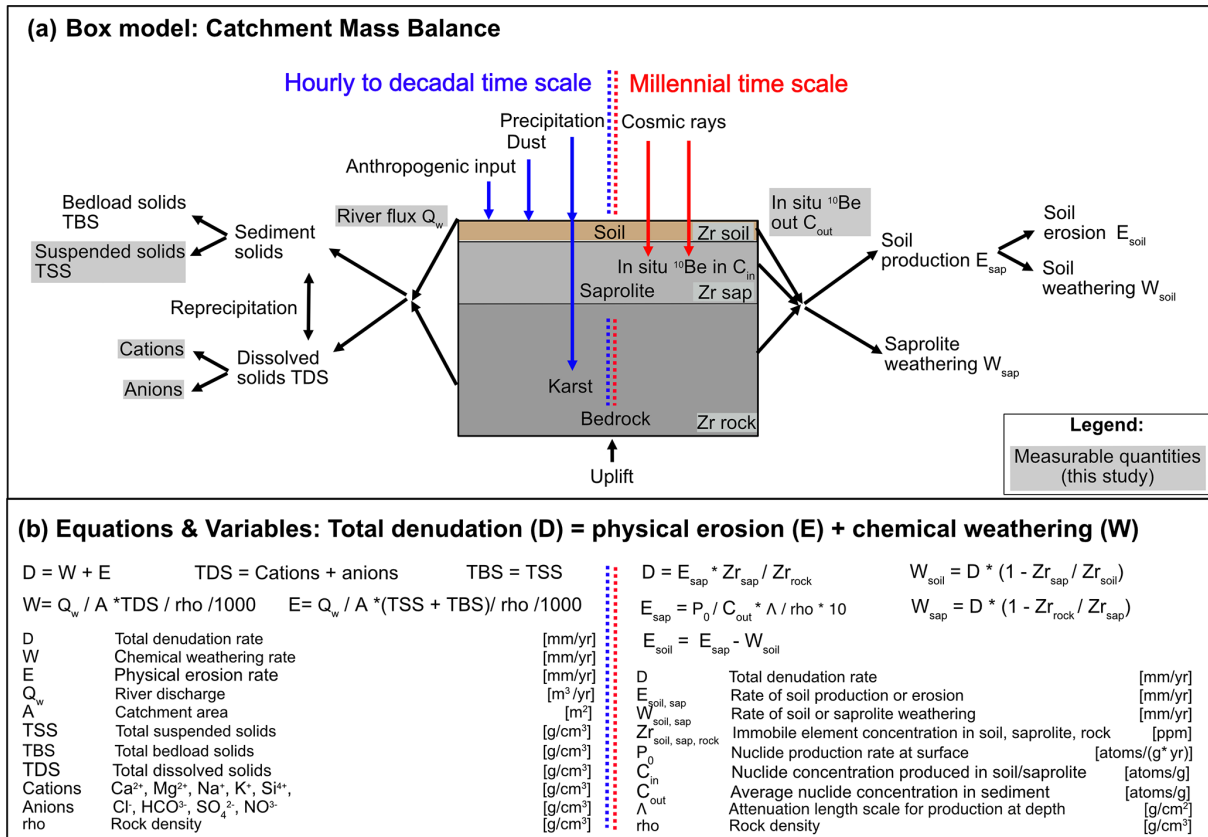


Figure 1. Approaches for the calculation of denudation rates. Schematic overview of two different approaches to determine chemical weathering and physical erosion and, hence, total denudation rates for river catchments. The method based on river load gauging integrates over hours or the last tens of years (left side). The method of in situ-produced denudation rate in combination with immobile elements integrates over tens of thousands of years (right side). **(a)** A box model indicating material fluxes and processes over these two timescales and **(b)** the equations applied to these timescales.

of different methods to quantify rates are subject to uncertainties, as most studies rely on integrating a number of measurements over diverse terrain to infer the overall system behavior.

In this study, we complement previous work by investigating decadal-timescale W and E using measurements of stream water chemistry, suspended solids, and river flow conditions. We do this with the aim of understanding the partitioning of W/D for adjacent catchments (and sub-catchments) in the same climate zone. More specifically, we investigate intermediate-sized river systems (71–12 710 km²) draining the Swabian Alb in southwestern Germany (Fig. 2). These rates are compared to millennial-timescale estimates of denudation from in situ-produced cosmogenic nuclides and other geologic constraints on escarpment retreat and landscape evolution. Lastly, we also calculate the horizontal retreat rates of escarpments in the study area, as these regions have higher slopes and may differ from catchment-averaged rates. The two rivers lie within a similar climate and ecologic zones but grade to different base levels and contain different compositions of layered carbonate, evaporite, and silici-

clastic lithologies in their individual sub-catchments (Fig. S1 in the Supplement). Specific questions we address include the following: (i) how do lithology and topography determine decadal-timescale W , E , and D in the context of driving escarpment retreat? (ii) How do these decadal-timescale rates compare to rates of landscape evolution over millennial timescales and longer timescales? (iii) How do values of W/D in the Swabian Alb compare to global values of W/D ? (iv) To what degree are anthropogenic disturbances to the catchments important for the determination of W and E ? The results and interpretations presented here suggest that lithologic (e.g., carbonate- and sulfate-bearing rocks) and base-level differences for catchments on either side of the continental drainage divide co-conspire to marked differences in chemical weathering rates. Anthropogenic disturbances in the catchments are significant but difficult to robustly quantify. However, after consideration of different approaches to correct for these disturbances, we find the previous interpretations remain the most likely outcome.

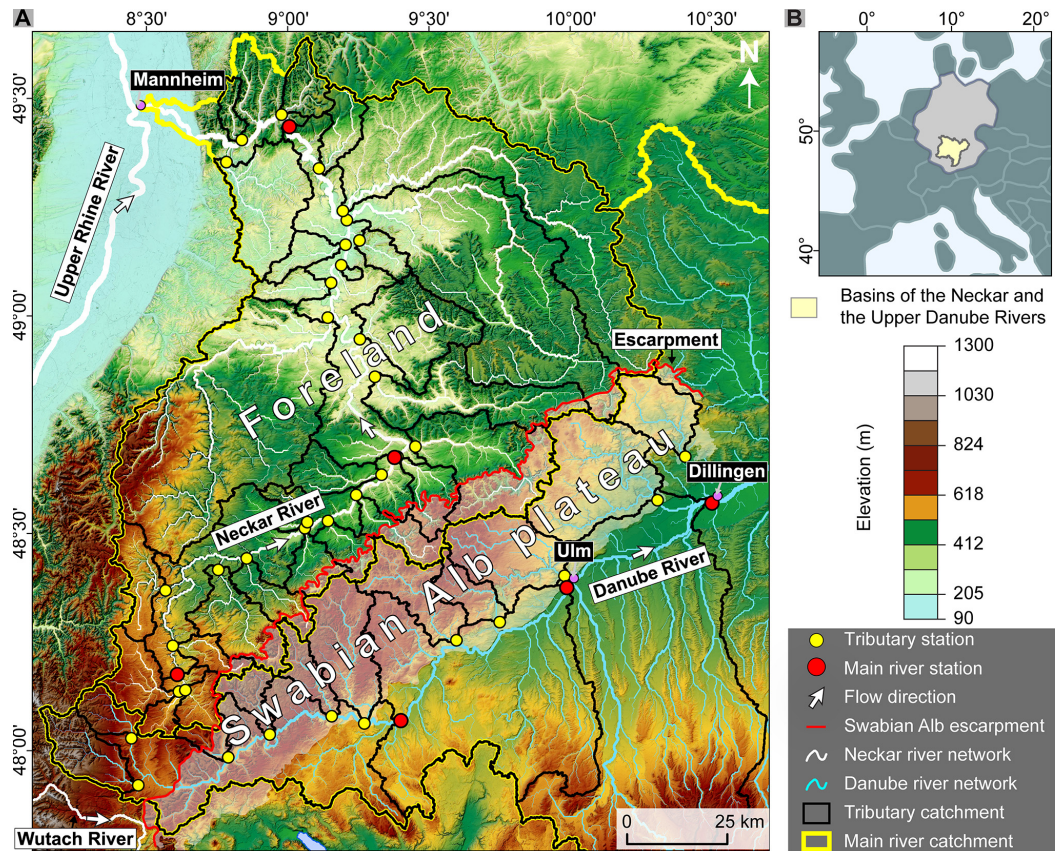


Figure 2. Overview of the study area: digital elevation model (DEM; LGL-BW ATKIS Digitales Geländemodell DGM 5 m, 2005) of the Swabian Alb escarpment area (southwestern Germany) with the two main drainage systems of the Neckar River draining the Rhine River northward in the northwest and with the Danube River draining to the southeast. The 200–400 m high escarpment is located on the northwestern side of the Swabian Alb plateau and coincides with the continental drainage divide between the Neckar and Danube rivers. To the southeast of this drainage divide, the plateau gently dips to the southeast towards the Danube River. The circles give locations of river measurement stations providing data to calculate physical erosion and chemical weathering rates. See the main text for the range of time periods covered by the observations used.

2 Background to the Swabian Alb

The Swabian Alb is a 200–400 m high, 40–70 km wide escarpment in southwestern Germany, extending approximately 220 km from southwest to northeast (Fig. 2). The escarpment is composed of Jurassic limestone bedrock that gently dips to the southeast ($0\text{--}7^\circ$), forming a tabular bench (e.g., Dongus, 2000; Thiebes, 2011; Ring and Bolhar, 2020). The Jurassic carbonates are the youngest preserved unit, which caps a 1–2 km thick package of alternating sandstone, evaporite, and carbonate stratigraphy (Littke et al., 2008). Triassic and early Jurassic deposits that underlie the escarpment encompass a variety of lithologies, including siliciclastic formations (e.g., Buntsandstein, Keuper sandstone, Opalinus clay), carbonates (e.g., Muschelkalk; Arietenkalk, Rifkalk), evaporites (e.g., Keuper gypsum), and pre-Mesozoic crystalline basement rocks (Fig. S1). The timing of uplift and subaerial exposure of the Swabian Alb is represented by an unconformity between the Jurassic carbonates and Ceno-

zoic sedimentary cover of the Molasse basin and isolated deposits of Bohnerz (pisolithic iron oxides) in karst fissures with late Eocene to Pleistocene mammal fossil assemblages (e.g., Ufrecht, 2008; Ufrecht et al., 2016). In the westernmost area of the Swabian Alb, paleosols of the Bohnerz formation indicate a > 5 Ma exposure of this surface based on cosmogenic ^3He concentrations (Hofmann et al., 2017).

In addition, the Swabian Alb escarpment acts as a significant continental drainage divide (Fig. 2). The divide separates rivers on the Swabian Alb that are incised into the Jurassic plateau and flow southeast into the Danube River and rivers that start near the escarpment front and flow northward through the Jurassic and Triassic foreland towards the Neckar River (subsequently joining the Rhine River; Fig. 2). These adjacent river systems exhibit contrasting base-level elevations, with the Neckar River's base level in Mannheim lying at 83 m above sea level, while the Danube River reaches 465 m in Ulm after a similar along-river distance. The continental drainage divide is characterized by a pronounced

cross-divide topographic asymmetry, implying present-day systematic southward divide mobility due to escarpment retreat (Winterberg and Willett, 2019). A combination of sediment provenance analysis and mapping of fluvial features suggests that the Rhine River and its tributaries have expanded at the expense of the Danube River and its tributaries since the development of the Upper Rhine Graben (Davis, 1899; Petit et al., 1996; Villinger, 1998; Ziegler and Fraefel, 2009). This transition of formerly Danubian areas to the Rhine River and its tributaries, such as the Neckar River, occurred through numerous discrete river capture events, several of which are well documented (Villinger, 1998; Petit et al., 1996; Ziegler and Fraefel, 2009; Strasser et al., 2010; Yanites et al., 2013).

Previous river load measurements of Q_w and TSSs (e.g., Fig. 1, left side) suggest a decadal-timescale erosion rate E spanning $0.004\text{--}0.011\text{ mm yr}^{-1}$ for both the Neckar River and the Danube River (Blöthe and Hoffmann, 2022; Schaller et al., 2001; DGJ, 2014, 2012). The reported weathering rate W in the Neckar River is estimated at approximately 0.020 mm yr^{-1} based on Q_w and TDSs (Schaller et al., 2001), while the denudation rate D , the combination of W and E , ranges from $0.023\text{--}0.027\text{ mm yr}^{-1}$ (Schaller et al., 2001). The decadal-timescale W from TDSs of small tributaries north of the Swabian Alb indicates lithology-specific W (e.g., Hinderer, 2006). The reported rates span 0.017 mm yr^{-1} for carbonate-rich Keuper sandstone to 0.038 mm yr^{-1} for clay-dominated Middle Jurassic lithologies. W from TDSs of the Wutach area, a Danube tributary captured by the Rhine River $\sim 18\text{ kyr}$ ago that cuts through basement, Triassic, and Jurassic rocks, ranges from 0.045 to 0.082 mm yr^{-1} , with rates exceeding 0.250 mm yr^{-1} for evaporite lithologies (Bauer, 1993). Similar high weathering rates for the Wutach area were also reported based on the paired cosmogenic nuclide method over millennial timescales (Ott et al., 2024). Springs in the middle Swabian Alb indicate an average W of 0.052 mm yr^{-1} (Hönle, 1991). Lower rates of 0.027 mm yr^{-1} are reported for Upper Jurassic rocks in the Neckar-draining area of Reutlingen/Tübingen (Holzwarth, 1980). These rates are comparable to W from the Aitrach River (0.028 mm yr^{-1}), a tributary of the Danube River draining Upper Jurassic rocks (Poppe, 1993).

Previous work suggests that decadal-timescale D values are generally below the millennial-timescale rates derived from cosmogenic nuclide analyses, which range between 0.055 and 0.135 mm yr^{-1} (Schaller et al., 2001, 2002). This has been attributed to a possible under-representation of high-magnitude, low-frequency events in decadal-timescale rates or spatially non-uniform denudation in millennial-timescale rates due to landslides along the escarpment during the Pleistocene (Terhorst, 2001). In addition, ^{10}Be -derived denudation rates only reflect erosion of quartz-bearing lithologies, such as Triassic sandstones exposed in the foreland of the Swabian Alb. Long-term rock uplift rates are closer to existing denudation rate estimates from river

loads. Periods of rock uplift above sea level are recorded by a regionally extensive early Miocene paleo-shoreline (cliff line) preserved along the southern edge of the Swabian Alb (0.05 mm yr^{-1} ; Hoffmann, 2017) and by locally preserved cave infills within the karstified limestone (0.01 mm yr^{-1} ; Strasser et al., 2009). Cave infills in the Upper Jurassic contain abundant terrestrial fossils that have been used to create a biostratigraphic record of karst evolution (Ufrecht et al., 2016). Cave levels increase in age, moving to higher elevations within the Swabian Alb, and fossil assemblages shift to more brackish and marine environments in these oldest deposits, reflecting the progressive lowering of regional base level during the late Cenozoic (Abel et al., 2002; Ufrecht et al., 2016).

3 Methods

To evaluate the denudation rate D for the Swabian Alb-draining rivers, lithologies and catchment-averaged metrics are extracted for 3 Neckar River locations, 26 Neckar tributaries, 3 Danube River locations, and 11 Danube tributaries draining the Swabian Alb. Neckar tributaries were separated into tributaries having a drainage divide with Danube tributaries on the Swabian Alb (12 tributaries called Neckar Swabian Alb tributary) and all remaining Neckar tributaries in the Swabian Alb foreland (14 Neckar foreland tributaries). Decadal-timescale W and E values are calculated from river Q_w and river load TDSs and TSSs for three different correction approaches described below. D is then transformed into Swabian Alb escarpment retreat rates, where applicable. TSS and TDS measurement stations are situated at the same location. However, the location of Q_w measurement stations may be in some cases at a slightly different location. The catchment-averaged metrics and the lithologies are extracted at the TDS and TSS locations. The time periods over which Q_w and river load TDSs and TSSs were available varied temporally and spatially due to data availability. In general, Q_w measurements were available from ~ 1940 to 2009, whereas river load TDSs and TSSs were available from ~ 1997 to 2020 (see Table S1 at <https://doi.org/10.5281/zenodo.13588248> (Schaller et al., 2024) for exact date ranges available for each sample location shown in Fig. 2).

3.1 Catchment-averaged topographic metrics, lithologies, and anthropogenic disturbances

Metrics extracted for the catchments encompass catchment area, mean elevation, local relief, hillslope angle, local channel slope normalized by upstream drainage area, mean annual precipitation, mean annual temperature, vegetation cover from NDVI, surface area by lithology, and anthropogenic influence. We utilized a 5 m digital elevation model (DEM) sourced from Baden-Württemberg's State Institute for the Environment (LGL-BW ATKIS Digitales Gelände-

modell DGM 5 m, 2005) to extract catchment metrics widely used to unravel patterns and rates of physical erosion and chemical weathering across diverse landscapes (e.g., Ahnert, 1970; Montgomery and Brandon, 2002; DiBiase et al., 2010; Portenga and Bierman, 2011; Harel et al., 2016). Catchments were extracted from the DEM with the TopoToolbox software (Schwanghart and Scherler, 2014), employing existing measurement stations (discharge, solute solids, and dissolved solids) as pour points. Local relief was determined as the elevation range within a 1.5 km diameter circular neighborhood (e.g., DiBiase et al., 2010; Peifer et al., 2021). The hillslope angle was computed by fitting a 3-by-3 cell plane for each DEM cell using the least-squares method. A comparison of local channel slope normalized by upstream drainage area and a regional reference concavity was calculated using the empirical power-law relationship between local channel slope (S) and upstream drainage area (A) (Eq. 1; Flint, 1974):

$$S = k_{sn} A^{-\theta_{ref}}. \quad (1)$$

A reference channel concavity (θ_{ref}) of 0.45 was used to compare a normalized fluvial relief (k_{sn}) across stream segments or watersheds with different drainage areas (Kirby and Whipple, 2012). The interpretation of k_{sn} is problematic in karstified landscapes such as the Swabian Alb due to substantial subsurface discharge, and we urge caution in overinterpreting variations in it. Nevertheless, we include it here for completeness, as it is commonly used in similar studies conducted in quartz-rich catchments and inclusion of it here provides a means for interested readers to compare it to other studies. The river network was extracted using an upslope area threshold for channel initiation of 1 km², and a smoothing window of 100 m was used to calculate local channel slope. We computed catchment-averaged k_{sn} to compare fluvial relief between basins with suspended sediment and solute load data (Forte and Whipple, 2019).

Catchment-averaged mean annual precipitation rates and mean annual temperature were extracted from the Climatologies at high resolution for the Earth's land surface areas (CHELSA) version 2 climatology dataset covering the years 1981–2010 (Karger et al., 2017, 2021). This dataset provides high-resolution (30 arcsec) estimates of precipitation and temperature derived from downscaled ERA-Interim climatic reanalysis. Vegetation cover was estimated using the Copernicus Land Monitoring Service's (CLMS's) long-term statistics of Normalized Difference Vegetation Index (NDVI) over the period between 1999–2019 (European Commission Directorate-General Joint Research Centre, 2021; León-Tavare et al., 2021). NDVI, defined as $NDVI = (NIR - Red)/(NIR + Red)$, relies on reflectance measurements in the near-infrared (NIR) and red (Red) bands. Soil thickness is provided by the worldwide data source DAAC (Pelletier et al., 2016).

Lithological data were extracted from the “General Geological Map of the Federal Republic of Germany” dataset, mapped at a scale of 1 : 250 000 (BGR, 2019). The extracted

lithologies are bundled into 10 bins distinguished by formation age, which are then further classified into three categories, including carbonates (Upper Jurassic), carbonates containing evaporites (Middle Triassic), and silicate (Proterozoic, and Paleozoic) together with siliciclastic lithologies (Lower and Upper Triassic, Lower and Middle Jurassic, Tertiary and Quaternary).

Anthropogenic impacts on each catchment were evaluated using three different main approaches. Firstly, the Connectivity Status Index (CSI) for river systems was evaluated for each catchment, where values of 100 % represent undisturbed rivers (Grill et al., 2019). Secondly, the Human Footprint Index (HFI) was extracted, with the highest impact being 50 and the lowest impact being 0 (Mu et al., 2022). This HFI represents the relative anthropogenic influence in each terrestrial biome and is represented as a percentage. Thirdly, the percentage of different land cover, such as artificial surfaces and constructions, along with cultivated area, vineyard, or tree covers, was extracted from the land cover map of Europe 2017 (Malinowski et al., 2020). The third metric used for anthropogenic impact is the percentage area of artificial constructions and surfaces.

3.2 Calculation of decadal-timescale rates from river load

A , Q_w , TSSs, and TDSs of rivers are used to calculate decadal-timescale E , W , and D values (Fig. 1, left side). TSS and TDS measurement stations are generally situated at the same location (Fig. 2). If there was no Q_w measurement station at the same location, the closest Q_w measurement station was selected (24 of total 43 locations; Table S1). The different datasets neither cover the same time periods nor contain the same number of data, nor was the collected sample material analyzed in the exact same way. Hence, the calculated rates need to be considered cautiously, as the results presented below are based on the average of the time series available. Data for the averages of daily Q_w and hourly Q_w are consolidated for the Neckar River (3 stations; DGJ, 2012) and some of its tributaries (26 stations; DGJ, 2012; LUBW, 2023) and for the Danube River (3 stations; DGJ, 2014) and some of its tributaries (11 stations; DGJ, 2014; LUBW 2023).

The calculation of W is based on the average Q_w and average TDS (Fig. 1 left side; single measurement of cations and anions every month for ~ 20 years) extracted from 29 stations for the Neckar River and tributaries (LUBW, 2023) and 13 stations for the Danube River and its Swabian Alb tributaries (LUBW, 2023; GKD, 2023). The TDS measurements generally comprise the total concentration of major cations (Ca^{2+} , Mg^{2+} , Na^+ , K^+ , and Si^{4+}), along with Cl^- , SO_4^{2-} , and HCO_3^- . Si^{4+} values were unavailable, and HCO_3^- concentrations were derived from reported pH and alkalinity (Cole and Prairie, 2014). To calculate W , measured TDSs can be corrected with different approaches, such as atmo-

spheric and anthropogenic inputs, and for secondary calcite precipitation. This study uses three approaches to calculate W (Table S2): (1) a simple rate W_{simple} corrected for 60 % atmospheric HCO_3^- (Katz et al., 1985); (2) $W_{\text{corr.}}$ corrected for atmospheric HCO_3^- , rain input (Agster, 1986), and attribution of all Cl^- to road salt; and (3) $W_{\text{sec. prec.}}$ which is based on the assumption that 90 % of the originally dissolved Ca^{2+} concentration reprecipitates (e.g., Erlanger et al., 2021) in addition to the correction $W_{\text{corr.}}$. We note that $W_{\text{sec. prec.}}$ is a maximum W , but we report this rate to show the effect of secondary calcite precipitation on W . The SO_4^{2-} concentration is considered to be entirely the weathering product of gypsum/anhydrite and not due to the oxidation of Fe sulfides in clay (e.g., Opalinus clay; Hinderer 2006). $W_{\text{corr.}}$ corrects for rain input, assuming that half of the catchment area is cultivated and the other half is forested. This assumption influences the correction of W for rain input only marginally, as rain input contributes generally less than 5 % to TDSs. $W_{\text{corr.}}$ provides a minimum rate, as NaCl attributed to road salt could also be released by rock salt, which is present in the Middle Triassic Muschelkalk formation. In contrast, $W_{\text{sec. prec.}}$ is considered a maximum rate, as a 90 % fraction of Ca reprecipitation is likely a maximum estimate (Erlanger et al., 2021), and some Ca is weathered from gypsum in the Muschelkalk and lower Keuper formations.

TSS measurements (single measurement every month for ~ 10 to 20 years) are less abundant than TDS data. TSS measurements, used as a proxy for the physical erosion rate E over these time intervals, are generally missing measurements during rare high- Q_w events and do not include bedload sediment fluxes. Three different erosion rates E are calculated to bracket these uncertainties using available TSSs, A , and Q_w (Fig. 1 left side; dataset S1 in the Supplement) and a sediment density of 2.7 g cm^{-3} : (1) E_{simple} is based on the average of all reported TSSs and the averaged Q_w , resulting in a minimum E ; (2) E_{RC} is estimated from hourly Q_w values and available corresponding TSSs using an empirical relation; and (3) a maximum rate $E_{\text{corr.}}$ is based on further correction of E_{RC} for an addition of bedload (Fig. 1 left side). This correction assumes that the total bedload TBS value equals the TSS value for sand-bedded rivers as indicated in the compilation of Turowski et al. (2010).

Three different values for D are reported based on previous approaches for calculating W and E . The different D values are reported for available measurement stations. (1) D_{simple} is the sum of E_{simple} and W_{simple} , representing an uncorrected D . (2) $D_{\text{corr.}}$ is a corrected D based on $E_{\text{corr.}}$ (the maximum E) and $W_{\text{corr.}}$ (the minimum W). $D_{\text{corr.}}$ is considered the most realistic D of the three. (3) $D_{\text{sec. prec.}}$ is the sum of $E_{\text{corr.}}$ and $W_{\text{sec. prec.}}$, suggesting a maximum D . Based on the different approaches, the contribution of W to D is reported by dividing W by D : (1) W/D_{simple} (W_{simple} over D_{simple}) resulting in maximum values for W/D , (2) $W/D_{\text{corr.}}$ ($W_{\text{corr.}}$ over $D_{\text{corr.}}$) representing a minimum value and considered to result in the most realistic values of the three,

(3) and values of $W/D_{\text{sec. prec.}}$ ($W_{\text{sec. prec.}}$ divided by $D_{\text{sec. prec.}}$) reporting values between W/D_{simple} and $W/D_{\text{corr.}}$.

The vertical $D_{\text{corr.}}$, which is considered the most realistic D , is transformed into a horizontal retreat rate for the Swabian Alb escarpment (Wang and Willett, 2021). These rates are derived from converting vertical denudation into horizontal retreat and are considered maximum values. More specifically, this was done by taking the denudation rate over the catchment area and applying the mass eroded per unit of time across the escarpment height in that catchment. This approach assumes all catchment denudation occurs along the escarpment and provides an upper bound on the retreat rate. The retreat rate is performed for one retreat direction (aspect), which is perpendicular to the mean orientation of the shared drainage divide between two adjacent and competing catchments. This was calculated along the entire length of the escarpment within each catchment. The retreat rates were further corrected by taking into account reduced denudation of the plateau area (Wang et al., 2021). Denudation of the plateau area is given by $D_{\text{corr.}}$ from the Danube Swabian Alb tributaries sharing catchment divides with the Neckar Swabian Alb tributaries.

In addition, $E_{\text{corr.}}$, $W_{\text{corr.}}$, and $D_{\text{corr.}}$ are analyzed for simple linear correlations with geomorphic, climatic/biotic, lithologic, and anthropogenic impact metrics. The reported correlation sets include (1) all data of the Neckar and Danube rivers and the tributaries, (2) the Neckar Swabian Alb tributaries, and (3) the Danube Swabian Alb tributaries.

4 Results

4.1 Decadal-timescale rates from river load

W_{simple} values from the Neckar River and its tributaries are highly variable and range over 2 orders of magnitude, from $0.005\text{--}0.084 \text{ mm yr}^{-1}$ (Fig. 3a and Table S3–S6). Tributaries draining the escarpment of the Swabian Alb show generally higher chemical weathering rates than the Neckar foreland tributaries that drain older Mesozoic bedrock units. W_{simple} values for the Danube River and its Swabian Alb tributaries are more homogenous and generally below 0.040 mm yr^{-1} (Fig. 3b). The observations made for W_{simple} are the same for $W_{\text{corr.}}$ further corrected for rain and road salt input (Fig. 4a and Table 1). The average $W_{\text{corr.}}$ for the Neckar Swabian Alb tributaries (0.044 mm yr^{-1}) is double the average rate for the Danube Swabian Alb tributaries (0.018 mm yr^{-1}). Similar trends are also visible for $W_{\text{sec. prec.}}$ but with values as high as 0.300 mm yr^{-1} for the Swabian Alb tributaries of the Neckar River and 0.160 mm yr^{-1} for the Swabian Alb tributaries of the Danube River. While $W_{\text{sec. prec.}}$ is considered a maximum rate, $W_{\text{corr.}}$ represents a minimum rate.

E_{simple} based on the average TSSs and Q_w of rivers ranges from below $0.001\text{--}0.003 \text{ mm yr}^{-1}$ for all analyzed rivers (Tables S6 and S7). In contrast, E_{RC} can be as high as 0.036 mm yr^{-1} for Neckar tributaries but is still

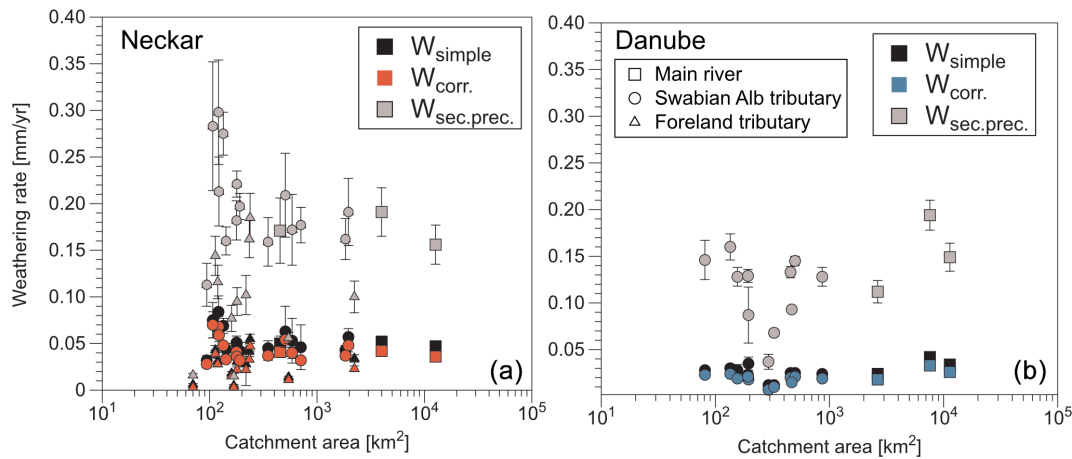


Figure 3. Decadal-timescale chemical weathering rates versus catchment area for (a) the Neckar River (squares), its foreland tributaries (triangles), and its Swabian Alb tributaries (circles) and (b) the uppermost reach of the Danube River (squares) and its Swabian Alb tributaries (circles). The values shown are the rates corrected for atmospheric HCO_3^- (W_{simple}), the rates corrected for rain and road salt input ($W_{\text{corr.}}$, a minimum scenario), and a rate considering additional secondary calcite precipitation ($W_{\text{sec.prec.}}$, a maximum scenario). Values for $W_{\text{corr.}}$ are considered the most reliable (see Methods). Values shown (and in Table 1) are not corrected for anthropogenic disturbances, which are addressed in Sects. 4.2 and 5.1.2.

low for the Danube River and its Swabian Alb tributaries ($0.000\text{--}0.002\text{ mm yr}^{-1}$; Fig. S2). Correction for bedload increases the $E_{\text{corr.}}$ in tributaries of the Neckar River to 0.072 mm yr^{-1} , whereas the Danube River and its Swabian Alb tributaries stay below 0.005 and 0.004 mm yr^{-1} , respectively (Fig. 4b). The resulting D_{simple} values range from $0.005\text{--}0.086\text{ mm yr}^{-1}$, the $D_{\text{corr.}}$ values range from $0.005\text{--}0.119\text{ mm yr}^{-1}$ (Fig. 4c), and $D_{\text{sec.prec.}}$ may be as high as 0.346 mm yr^{-1} (Table S6). The main general trend is that the rates of Neckar tributaries are more heterogeneous and higher than values from the Danube and its Swabian Alb tributaries (Fig. 4c).

Comparing the fraction of chemical weathering on total denudation (Table S6), W/D_{simple} shows little variability (values between 0.94 and 1.00). $W/D_{\text{corr.}}$, based on corrections of rain and road salt, yields the strongest spread in values, and $W/D_{\text{sec.prec.}}$ shows some outliers for the Neckar tributaries (Fig. 5). Generally, W/D values range from 0.40 to almost 1.00 for the Neckar tributaries and from 0.70–0.99 for Danube Swabian Alb tributaries. Escarpment retreat rates based on basin projection and $D_{\text{corr.}}$ range from 1.0–8.1 mm (average: 3.3 mm yr^{-1} ; Table 2). Retreat rates, which consider lower denudation rates of plateau areas, are only slightly lower (average: 2.9 mm yr^{-1}).

4.2 Correlation of catchment metrics with denudation rates

Statistically significant linear correlations with rates ($W_{\text{corr.}}$, $E_{\text{corr.}}$, and $D_{\text{corr.}}$) for all investigated catchments are reported for only a few metrics (Tables 3 and S8–S12 and Figs. S3–S6). The corresponding P values for all correlations reported here are $P < 0.05$. Furthermore, for brevity, simple linear re-

gressions are not reported for all combinations of rates and metrics, and we instead focus on the most meaningful results from the exercise. Results indicate $W_{\text{corr.}}$ has a moderate inverse correlation with the mean annual precipitation ($R = -0.40$), some lithologies and anthropogenic impact, but no topographic metrics. $W_{\text{corr.}}$ shows a moderate positive correlation with anthropogenic disturbances suggested by HFI ($R = 0.49$) and the area of artificial constructions ($R = 0.52$) but is not significantly correlated with CSI. While the abundance of the Lower Triassic lithologies (e.g., sandstone) correlates inversely, the Upper Triassic (e.g., sandstone and marl), Lower Jurassic (e.g., claystone), and Middle Jurassic (e.g., claystone) lithologies positively correlate with $W_{\text{corr.}}$. $E_{\text{corr.}}$ shows positive and moderate correlations with maximum relief ($R = 0.44$), the Lower Jurassic ($R = 0.46$), and the Middle Jurassic ($R = 0.35$). In addition, $E_{\text{corr.}}$ correlates inversely with CSI ($R = -0.55$) and positively with artificial constructions ($R = 0.52$). $D_{\text{corr.}}$ indicates positive moderate correlations with maximum relief ($R = 0.41$) and a negative correlation with mean annual precipitation ($R = -0.40$). $D_{\text{corr.}}$ correlates negatively with the Lower Triassic (e.g., sandstone) and positively with the Lower and Middle Jurassic (e.g., claystone). Furthermore, correlation of $D_{\text{corr.}}$ is observed with CSI ($R = -0.52$), HFI ($R = 0.52$), and artificial constructions ($R = 0.66$).

$W_{\text{corr.}}$ of the Neckar Swabian Alb tributaries (Tables 3 and S11) correlates strongly and inversely with the maximum relief ($R = -0.83$). In addition, $W_{\text{corr.}}$ correlates positively with the percentage of the lithology for the Lower Jurassic (e.g., claystone). A significant negative correlation was found for $E_{\text{corr.}}$ with CSI ($R = -0.63$). In the case of the Danube Swabian Alb tributaries (Tables 3 and S12), a

Table 1. Compilation of chemical weathering, physical erosion, and total denudation rates for the Swabian Alb. Values reported are not corrected for anthropogenic impact (see Sects. 4.2 and 5.1.2) aside from rain and road salt corrections and are based on the procedures described in Sect. 3.2.

River	Location ¹	N ¹ °	E ¹ °	Area km ²	W _{corr.} ² mm yr ⁻¹	E _{corr.} ³ mm yr ⁻¹	D _{corr.} ⁴ mm yr ⁻¹	W/D _{corr.} ⁵
Neckar								
Neckar	Rottweil	48.17809	8.62060	461	0.041	0.009	0.050	0.82
Neckar	Wendlingen	48.67732	9.37105	3049	0.042	0.010	0.053	0.81
Neckar	Rockenau	49.43178	9.00608	12647	0.036			
Mean Neckar					0.040	0.010	0.051	0.81
Neckar tributaries ⁶								
<i>Eschach</i>	<i>Rottweil</i>	<i>48.13876</i>	<i>8.62609</i>	<i>217</i>	<i>0.022</i>	<i>0.001</i>	<i>0.023</i>	<i>0.94</i>
Prim	Rottweil, Altstadt	48.14255	8.64767	121	0.068	0.008	0.076	0.89
Schlichem	Epfendorf	48.24372	8.60330	110	0.070			
<i>Glatt</i>	<i>Hopfau</i>	<i>48.37126</i>	<i>8.57827</i>	<i>216</i>	<i>0.033</i>	<i>0.003</i>	<i>0.037</i>	<i>0.91</i>
Eyach	Mühlingen	48.41900	8.75995	347	0.037	0.043	0.080	0.47
Starzel	Bieringen	48.44556	8.85812	178	0.041	0.030	0.071	0.58
Steinlach	Tübingen	48.51550	9.05920	143	0.033	0.003	0.036	0.93
<i>Ammer</i>	<i>Lustnau</i>	<i>48.52909</i>	<i>9.06789</i>	<i>162</i>	<i>0.047</i>	<i>0.001</i>	<i>0.048</i>	<i>0.98</i>
Echaz	Kirchentellinsfurt	48.53152	9.13923	135	0.048	0.072	0.119	0.40
Erms	Neckartenzlingen	48.59104	9.23763	179	0.036	0.004	0.040	0.91
<i>Aich</i>	<i>Oberensingen</i>	<i>48.63758</i>	<i>9.32513</i>	<i>179</i>	<i>0.022</i>	<i>0.010</i>	<i>0.032</i>	<i>0.69</i>
Lauter	Wendlingen	48.67874	9.38075	192	0.032	0.004	0.036	0.90
Fils	Plochingen	48.70216	9.44380	695	0.032	0.015	0.047	0.69
Rems	Plüderhausen	48.86285	9.30332	575	0.040	0.010	0.051	0.79
<i>Murr</i>	<i>Murr-Mündung</i>	<i>48.94955</i>	<i>9.25137</i>	<i>506</i>	<i>0.054</i>	<i>0.012</i>	<i>0.067</i>	<i>0.81</i>
<i>Enz</i>	<i>Besigheim</i>	<i>48.99929</i>	<i>9.13966</i>	<i>2214</i>	<i>0.023</i>	<i>0.022</i>	<i>0.045</i>	<i>0.51</i>
<i>Zaber</i>	<i>Lauffen, Zaber</i>	<i>49.07917</i>	<i>9.15174</i>	<i>115</i>	<i>0.039</i>	<i>0.000</i>	<i>0.040</i>	<i>0.99</i>
<i>Schozach</i>	<i>Heilbronn</i>	<i>49.11986</i>	<i>9.18743</i>	<i>94</i>	<i>0.028</i>			
<i>Lein</i>	<i>Heilbronn</i>	<i>49.16677</i>	<i>9.20299</i>	<i>115</i>	<i>0.028</i>			
<i>Sulm</i>	<i>Binswangen</i>	<i>49.17688</i>	<i>9.25182</i>	<i>103</i>	<i>0.059</i>			
Kocher	Kochendorf	49.22325	9.20766	1966	0.048	0.016	0.064	0.75
Jagst	Jagstfeld	49.24538	9.19325	1834	0.037	0.005	0.042	0.89
<i>Elz</i>	<i>Neckarelz</i>	<i>49.34209</i>	<i>9.10970</i>	<i>159</i>	<i>0.015</i>			
<i>Itter</i>	<i>Eberbach</i>	<i>49.46611</i>	<i>8.97817</i>	<i>155</i>	<i>0.003</i>	<i>0.001</i>	<i>0.005</i>	<i>0.73</i>
<i>Steinach</i>	<i>Neckarsteinach</i>	<i>49.40799</i>	<i>8.83807</i>	<i>69</i>	<i>0.003</i>			
<i>Elsenz</i>	<i>Bammental</i>	<i>49.35797</i>	<i>8.78512</i>	<i>509</i>	<i>0.011</i>	<i>0.002</i>	<i>0.014</i>	<i>0.83</i>
Mean Neckar tributaries					0.035	0.013	0.049	0.78
Mean Neckar Swabian Alb tributaries					0.044	0.019	0.060	0.74
Danube								
Danube	Hundersingen	48.07238	9.39654	2629	0.018	0.004	0.022	0.82
Danube	Neu-Ulm	48.37389	9.96427	7588	0.033			
Danube	Dillingen	48.56833	10.50016	11346	0.026			
Mean Danube					0.025	0.004	0.022	0.82
Danube Swabian Alb tributaries								
Breg	Hüfingen	47.92297	8.48861	269	0.007	0.003	0.010	0.70
Brigach	Marbach	48.03079	8.46432	135	0.018	0.002	0.020	0.88
Elta	Tuttlingen	47.98806	8.79634	81	0.023	0.001	0.024	0.96
Bära	Hammerschmiede	48.04055	8.93825	132	0.024	0.002	0.026	0.92
Schmeie	Inzigkofen	48.08270	9.14974	153	0.019	0.002	0.021	0.91
Lauchert	Sigmaringendorf	48.06546	9.26340	454	0.020	0.002	0.022	0.91
Grosse Lauter	Lauterach	48.25587	9.58009	324	0.010	0.001	0.012	0.89
Schmiech	Ehingen	48.29686	9.73059	167	0.021	0.001	0.021	0.96
Blau	Ulm-Söflingen	48.40184	9.95565	486	0.021			
Brenz	Bergenweiler	48.57240	10.28102	755	0.019	0.001	0.020	0.95
Egau	Dischingen	48.67148	10.37964	284	0.015			
Mean Danube Swabian Alb tributaries					0.018	0.002	0.020	0.90

¹ Location and coordinates (WGS84) of measurement stations for dissolved and suspended solids. ² Chemical weathering rate $W_{\text{corr.}}$ corrected for atmospheric HCO_3^- and input by rain and road salt. ³ Physical erosion rate $E_{\text{corr.}}$ corrected for rating curve and bedload assuming that bedload equals suspended load.

⁴ $D_{\text{corr.}}$ based on $E_{\text{corr.}}$ and $W_{\text{corr.}}$. ⁵ $W/D_{\text{corr.}}$ based on $W_{\text{corr.}}$ over $D_{\text{corr.}}$. ⁶ Rivers in italics are foreland tributaries of the Neckar River.

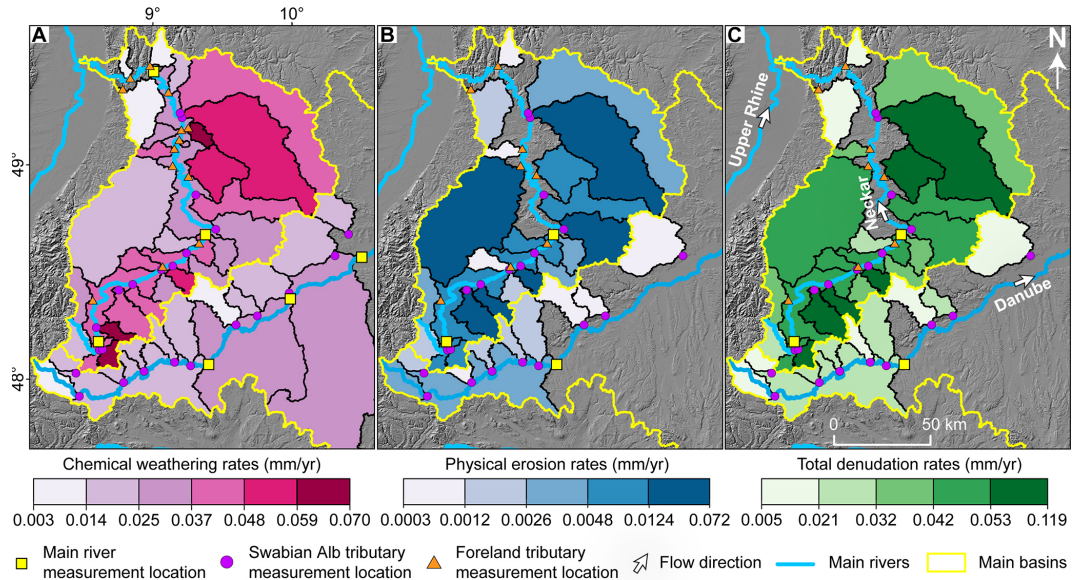


Figure 4. Mean spatial decadal-timescale denudation rates: maps (LGL-BW ATKIS Digitales Geländemodell DGM 5 m, 2005) showing calculated rates in catchments of the Neckar River and Upper Danube River and their tributaries. (a) W_{corr} , derived from dissolved solids. (b) E_{corr} , from suspended load and bedload. (c) D_{corr} , as the sum of E_{corr} and W_{corr} . See Table 1 for values plotted.

Table 2. Escarpment retreat rates of the Swabian Alb based on the approach of basin projection provided by Wang and Willett (2021) and Wang et al. (2021).

River			River			Aspect °	Basin projection ² mm yr ⁻¹	Basin projection ³ mm yr ⁻¹
D_{corr}^1 mm yr ⁻¹			D_{corr}^1 mm yr ⁻¹					
Neckar tributaries			Danube tributaries					
Prim	Rottweil, Altstadt	0.076	Elta	Tuttlingen	0.024	135.0	2.3	2.3
Schlichem	Epfendorf		Bära	Hammerschmiede	0.026	135.0		
Eyach	Mühringen	0.080	Schmeie	Inzigkofen	0.021	135.0	3.9	3.8
Starzel	Bieringen	0.071	Lauchert	Sigmaringendorf	0.022	135.0	2.7	2.6
Steinlach	Tübingen	0.036	Lauchert	Sigmaringendorf	0.022	157.5	1.1	1.0
Echaz	Kirchentellinsfurt	0.119	Grosse Lauter	Lauterach	0.012	135.0	3.6	3.3
Erms	Neckartenzlingen	0.040	Schmiech	Ehingen	0.021	135.0	1.5	1.1
Lauter	Wendlingen	0.036	Schmiech	Ehingen	0.021	180.0	1.3	1.0
Fils	Plochingen	0.047	Brenz	Bergenweiler	0.020	157.5	3.2	2.8
Rems	Remsmühle	0.051	Brenz	Bergenweiler	0.020	157.5	3.3	3.3
Kocher	Kochendorf	0.064	Brenz	Bergenweiler	0.020	180.0	8.1	8.1
Jagst	Jagstfeld	0.042				180.0	5.8	
Mean		0.060			0.021	151.9	3.3	2.9

¹ D_{corr} , based on W_{corr} and E_{corr} . ² Retreat rate based on basin projection method and D_{corr} . ³ Retreat rate based on basin projection method with correction for low D_{corr} of plateau area.

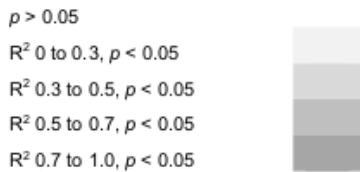
moderate to strong positive correlation for W_{corr} and HFI is reported ($R = 0.63$). Positive strong correlations of E_{corr} and mean elevation ($R = 0.82$), maximum relief ($R = 0.82$), and mean annual precipitation ($R = 0.79$) were found. E_{corr} has a strong inverse correlation with the mean annual temperature ($R = -0.87$) and cultivated areas ($R = -0.75$). No meaningful correlation of D_{corr} with any metric was observed for the Danube Swabian Alb tributaries.

5 Discussion

The Discussion is organized into three sections, exploring (i) the decadal-timescale chemical weathering W , physical erosion E , and total denudation rates D across all datasets, with an emphasis on tributaries of the Neckar River and Danube River within the Swabian Alb and also anthropogenic disturbances; (ii) the total denudation rates D observed in the Swabian Alb with rates documented in other studies spanning various longer timescales; and (iii) a discus-

Table 3. Pearson correlation coefficient between corrected rates and mean catchment metrics, given for all data and for the Neckar and Danube Swabian Alb tributaries.

	All data			Neckar Swabian tributaries			Danube Swabian tributaries		
	$W_{corr.}$ $n=43$	$E_{corr.}$ $n=32$	$D_{corr.}$ $n=32$	$W_{corr.}$ $n=12$	$E_{corr.}$ $n=11$	$D_{corr.}$ $n=11$	$W_{corr.}$ $n=11$	$E_{corr.}$ $n=9$	$D_{corr.}$ $n=9$
Catchment area	0.03	0.05	0.07	-0.15	-0.22	-0.19	-0.11	-0.19	-0.20
Mean elevation	0.17	-0.14	-0.28	0.54	0.15	0.27	-0.11	0.82	-0.11
Max. relief	0.07	0.44	0.41	-0.83	0.08	-0.28	-0.30	0.82	-0.50
Local relief (1000m)	0.09	0.23	0.09	-0.26	0.24	0.08	0.15	0.38	0.23
Trunk mean k_{gn}	0.22	0.20	0.01	-0.37	0.13	-0.08	0.02	0.56	0.02
Slope	0.07	0.21	0.09	-0.25	0.25	0.10	0.05	0.49	0.10
Mean annual precipitation	0.40	-0.25	-0.40	-0.10	-0.43	-0.52	-0.55	0.79	-0.55
Mean annual temperature	0.22	0.16	0.31	-0.57	-0.12	-0.25	0.18	-0.87	0.18
NDVI (Vegetation cover)	0.05	0.00	-0.03	0.29	-0.17	-0.05	-0.41	0.49	-0.31
Soil depth	0.20	-0.08	0.11	0.57	-0.11	0.12	-0.30	-0.17	-0.48
Connectivity Status Index	0.20	-0.55	-0.52	0.19	-0.63	-0.57	-0.24	-0.08	-0.21
Human Footprint Index	0.49	0.26	0.52	-0.19	0.22	0.27	0.63	-0.43	0.60
Artificial constructions	0.52	0.52	0.66	-0.07	0.51	0.51	0.41	-0.03	0.40
Cultivated area/vineyards	0.22	-0.07	0.11	-0.32	-0.17	-0.26	0.12	-0.75	0.01
LowerTriassic	0.44	-0.11	-0.31						
MiddleTriassic	0.12	-0.11	0.01	0.04	-0.12	-0.09			
UpperTriassic	0.47	0.11	0.35	0.21	-0.11	0.04			
LowerJurassic	0.62	0.46	0.63	0.74	0.18	0.41			
MiddleJurassic	0.41	0.35	0.44	0.06	0.13	0.10			
UpperJurassic	0.30	-0.13	-0.28	-0.43	0.04	-0.14	0.27	-0.42	0.25
Tertiary	0.26	-0.16	-0.25				0.00	-0.53	0.03
Quaternary	0.11	0.09	0.15	-0.60	0.00	-0.19	0.55	-0.22	0.55



sion of the contribution of chemical weathering and physical erosion to total denudation rates, leveraging global datasets and employing diverse methodologies to ascertain rates.

5.1 Decadal-timescale rates versus catchment metrics

5.1.1 Interpretation of calculated rates

In general, the W_{simple} and rain-/salt-corrected decadal-timescale $W_{corr.}$ calculations from all Neckar tributaries (Figs. 3a and 4a; average 0.035 mm yr^{-1}) agree well with decadal-timescale rates reported from small catchments in the Swabian Alb foreland and the Swabian Alb itself (e.g., Hinderer, 2006). These published rates range from 0.017 mm yr^{-1} for carbonate-rich sandstone to 0.038 mm yr^{-1} for carbonate-rich claystone and $> 0.250 \text{ mm yr}^{-1}$ for evaporites. The average of chemical weathering rates from these small catchments is comparable to $W_{corr.}$ for larger catchments in this study, which contain a mix of these same lithologies. In contrast, the corrected rates $W_{corr.}$ for the Neckar River are higher than the corrected weathering rates of Schaller et al. (2001), which may result from different datasets (e.g., time span and frequency of measurements). The possible correction for secondary cal-

cite precipitation and anthropogenic influences on carbonate weathering (e.g., Zeng et al., 2019) introduce additional uncertainties in W .

The $E_{corr.}$ rates (Fig. 4b) for the Neckar River are comparable to published rates of $\sim 0.010 \text{ mm yr}^{-1}$ (Blöthe and Hoffmann, 2022; DGJ, 2014) and $\sim 0.005 \text{ mm yr}^{-1}$ (Schaller et al., 2001). In contrast, $E_{corr.}$ values for the Danube River and its Swabian Alb tributaries are smaller than the already relatively low value of 0.005 mm yr^{-1} for the Danube River (DGJ, 2014; Fig. 4b). $E_{corr.}$ assumes that sediment load measurements capture a representative distribution of Q_w during the measurement period, but this is likely under sample-infrequent high-magnitude events that contribute high suspended and bedload sediment fluxes relative to solute loads (Pratt-Sitaula et al., 2007; Turowski et al., 2010). In addition, many TSS values decreased in major German rivers ($2000\text{--}160\,000 \text{ km}^2$) over the last ~ 20 years by up to 50 % (Hoffmann et al., 2023). Such a decrease in TSSs is generally observed in the Northern Hemisphere due to dams (Dethier et al., 2022). While intensively cultivated small catchments ($< 1 \text{ km}^2$) may report TSS values more than 40 times higher than pristine catchments (Vanmaercke et al., 2015), such an increase is not observed for larger catchments ($> 1000 \text{ km}^2$).

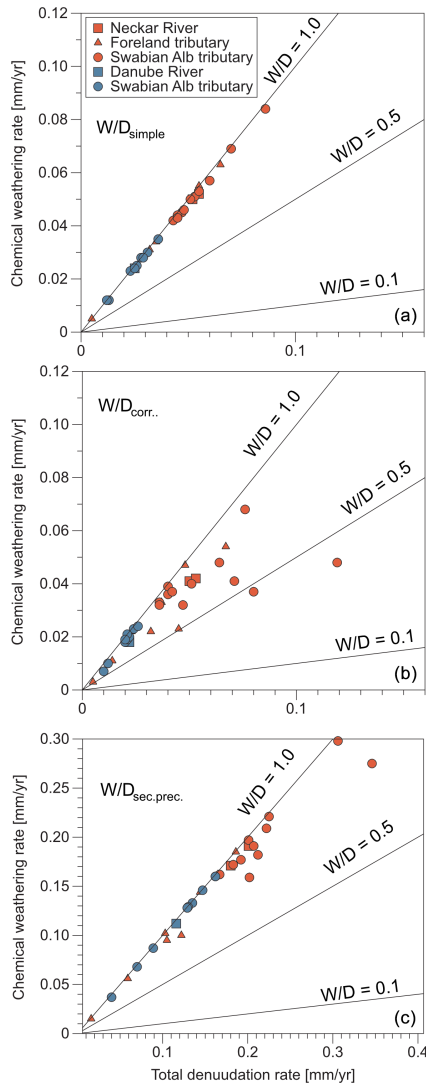


Figure 5. Effect of different corrections applied to the decadal-timescale rates: chemical weathering rate versus total denudation rate for the Neckar River and foreland and its Swabian Alb tributaries and for the Danube River and its Swabian Alb tributaries. (a) Uncorrected rates W_{simple} and D_{simple} , (b) correction of chemical weathering rates for rain and road salt input ($W_{\text{corr.}}$) and $D_{\text{corr.}}$, (c) correction of chemical weathering rate for secondary calcite precipitation ($W_{\text{sec.prec.}}$) and $D_{\text{sec.prec.}}$. See Sect. 3.2 for a description of the different correction approaches.

Despite all these uncertainties, a relative comparison shows that E values in the Neckar Swabian Alb tributaries are at least 2 times higher than rates from the Danube Swabian Alb tributaries (Fig. 4b). In general, the total denudation rates ($D_{\text{corr.}}$), which correspond to a composite of W and E , seem to be at least 2 times higher in the Neckar Swabian Alb tributaries than in the Danube Swabian Alb tributaries and in the Swabian Alb foreland tributaries (Fig. 4c).

5.1.2 Correction of rates for anthropogenic impact

Our correlation analysis between river load rates and various catchment metrics indicates that anthropogenic impact significantly influences calculated W , E , and D (Table 3 and Figs. S3–S6). Linear correlations between rates and anthropogenic impact metrics are as strong as, or even stronger than, those observed with lithological and geomorphic variables. A comparison between the Neckar and Danube Swabian Alb tributaries using three anthropogenic metrics – the Connectivity Status Index (CSI), the Human Footprint Index (HFI), and the percentage of artificial surfaces – highlights more intense anthropogenic impact in the Neckar than the Danube Swabian Alb tributaries (Table S13; see also Methods 3.1). For example, CSI values are on average lower on the Neckar side (99.16 %) than on the Danube side (99.54 %), indicating more disrupted river connectivity in the Neckar Swabian Alb tributaries. Similarly, HFI values are significantly higher on the Neckar side (29.59 %) than on the Danube side (25.19 %), and artificial surface coverage is also more extensive on the Neckar side (9.7 %) compared to the Danube side (5.2 %). All differences are statistically significant ($p < 0.05$), confirming a consistently stronger anthropogenic footprint in the Neckar than the Danube Swabian Alb tributaries.

To account for these differences, we propose recalculating river load rates by weighting them according to the level of anthropogenic impact. Specifically, $W_{\text{corr.}}$, $E_{\text{corr.}}$, and $D_{\text{corr.}}$ values were adjusted using CSI, HFI, and the percentage of artificial surface area (Table S13). The following weighting formulas were applied:

- CSI-weighted rate = Rate (Table 1) \times (CSI_{mean}/100), where 100 represents a fully undisturbed river system.
- HFI-weighted rate = Rate (Table 1) \times (1 – (HFI_{mean}/50)), where 50 is the maximum possible HFI and higher values denote more human impact.
- Artificial weighted rate = Rate (Table 1) \times (1 – (Artificial_{mean}/100)), where 100 corresponds to complete artificial land cover.

These corrections are based on the assumption that anthropogenic impacts, such as urbanization and mining, typically enhance both physical erosion and chemical weathering by removing vegetation, increasing surface runoff, and promoting contact with reactive agents (e.g., acid mine drainage, polluted urban runoff), among other effects. As such, catchments with higher anthropogenic impact will yield lower adjusted rates than their uncorrected values. Given that the Neckar Swabian Alb tributaries show consistently higher anthropogenic impact, the corrected rates for Neckar Swabian Alb tributaries are generally lower than the uncorrected ones, especially when compared to the Danube side. Among the three correction factors considered, the most substantial adjustments occur with the HFI correction ($D_{\text{HFI}}/D_{\text{corr.}} =$

0.71), whereas the CSI correction yields the smallest change ($D_{\text{CSI}}/D_{\text{corr.}} = 0.99$) (Table S13). The positive correlation between HFI and artificial constructions with denudation rates and the negative correlation with CSI, when all data are considered (Table 3), support the argument that natural rates are lower than the anthropogenically influenced ones. We acknowledge, however, that not all human impacts increase erosion rates; for instance, dam construction may reduce downstream sediment transport and thus lower physical erosion, in which case the adjustment for applying a correction to denudation rates should be reversed.

In summary, the proposed corrections are intentionally simplified, are non-process-based, and assume a linear relationship between anthropogenic impact and river load rates. While it remains uncertain which correction method best reflects real-world conditions, our approach offers a starting point for incorporating human impact into denudation rate calculations. Importantly, regardless of the correction method applied, W , E , and D in the Neckar Swabian Alb tributaries remain at least twice as high as those in the Danube Swabian Alb tributaries (Table S13). This pattern is consistent even in the uncorrected data (Table 1), indicating a robust signal of elevated rates in the Neckar Swabian Alb tributaries despite the uncertainties surrounding anthropogenic corrections.

5.1.3 Interpreted drivers of differences in rates and impact on escarpment retreat

We interpret the remaining differences in W , E , and D between the Neckar Swabian Alb tributaries and Danube Swabian Alb tributaries to reflect the contrast in base level between the two main catchments. These base-level differences were set by the reorganization of major river systems since the evolution of the Upper Rhine Graben and the onset of long-wavelength uplift in the Middle Miocene (e.g., Ring and Bolhar, 2020). We reason that the contrast in base level can affect W , E , and D in two ways. A lower base level on the Neckar side of the escarpment (1) increases topographic relief to drive E and W of the subsurface (via flow in karst) and (2) exposes layered stratigraphy with a range of susceptibilities to E and W . The climate is comparable on the two sides of the Swabian Alb, and the nearly flat-lying Mesozoic strata indicate that differential uplift is minor across the spatial scales of the catchments analyzed, so we focus our discussion on differences in lithology and relief across the escarpment and their controls on E and W .

The steep north-facing escarpment is drained by the Neckar Swabian Alb tributaries eroding the Upper Jurassic caprock and underlying easily erodible rock units of the Middle and Lower Jurassic (Fig. S1). In contrast, roughly two-thirds of the area of the Danube Swabian Alb tributaries exposes Upper Jurassic carbonates, and exposure of Middle and Lower Jurassic rock is confined to incised valleys (Fig. S1). The occurrence of Lower and Middle Jurassic rock units cor-

relates strongly with W , E , and hence D , which is seen in the Neckar Swabian Alb tributaries (Fig. S6 and Table 3). A strong correlation of W with the two lithologies may be attributed to claystone at the base of the Middle Jurassic (Fig. S6). These claystone units are known to be rich in pyrite (e.g., Hinderer, 2006), which enhances chemical weathering by the release of sulfuric acid (Fig. S7; e.g., Ross et al., 2018). Additionally, these clay units swell and disaggregate when wetted, potentially enhancing physical erosion (Thury, 2002). In this view, the steep topography of the escarpment could be coupled with the higher physical and chemical denudation rates of weak bedrock at the base of the escarpment, which facilitates escarpment retreat. Relief across the escarpment and between valleys of the Danube tributaries drives karstification of the Upper Jurassic caprock in both the Neckar Swabian Alb tributaries and the Danube Swabian Alb tributaries, which show a dominance of chemical weathering, and a 2-fold contrast in mean rates across the escarpment.

The escarpment retreat rates, calculated using river load and the basin projection method, range between 1.0 and 8.1 mm yr⁻¹ (Table 2). However, some measurement sites, such as those for the Kocher and Jagst rivers, are problematic. In these two cases, since the escarpment constitutes only a minor part of the large catchment area, transforming river load into horizontal retreat rates results in a maximum rate. The Swabian Alb escarpment's retreat rates are significantly faster than the global average of 0.6 mm yr⁻¹ (He et al., 2024) but agree reasonably well with rates of 2–10 mm yr⁻¹ compiled from all around the world (e.g., Duszyński et al., 2019). The relatively rapid retreat rates are likely due to the contrasting base-level elevations between the Neckar and Danube rivers (e.g., Villingner, 1998; Winterberg and Willett, 2019) and the exposure of easily physical and chemically erodible rock units below the Upper Jurassic cap rocks (e.g., claystone). This lithological contrast and elevation difference affects the geometry of these neighboring river systems, with the Neckar River basin growing as the Danube River basin shrinks.

5.2 Evaluation of spatial and temporal variations in rates

Despite integrating over short timescales, the higher decadal-timescale rates from the Neckar River and its Swabian Alb tributaries than the Danube River and its Swabian Alb tributaries, along with the escarpment retreat, are reflected in longer-timescale surface change rates (Fig. 6 and Table S14a and b). The decadal-timescale total denudation rate ($D_{\text{corr.}}$) for the Danube Swabian Alb tributaries (Fig. 6, blue left-pointing triangles) agrees with millennial-timescale rates based on in situ-produced cosmogenic ¹⁰Be in the uppermost reaches of the Danube River (Morel et al., 2003; blue diamonds in Fig. 6). Comparable millennial-timescale rates from a Danube Swabian Alb tributary are calculated from cave and terrace incisions (Abel et al., 2002; blue dots in Fig. 6). In addition, the decadal-timescale rates agree with

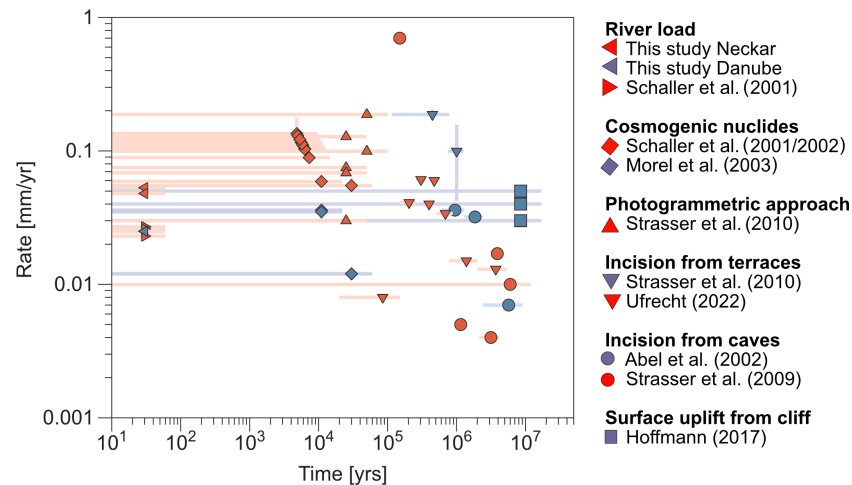


Figure 6. Synopsis of temporal variations in denudation rates: compilation of rates integrating over different timescales for locations north (red) and south (blue) of the present-day drainage divide of the Swabian Alb. The list of rates ranges from decadal-timescale rates from river load to million-year-scale rates based on the uplift of the cliff line in the Swabian Alb.

uplift rates integrating over the last 17.5 million years (Hoffmann, 2017; blue squares in Fig. 6). However, the rates determined from cave and terrace incision (e.g., Abel et al., 2002 (blue dots in Fig. 6); Strasser et al., 2009 (red dots in Fig. 6); Ufrecht, 2022 (downward-pointing red triangles in Fig. 6)) show local pulses of incision that can exceed rates averaged over million-year timescales or spatial scales of $> 10 \text{ km}^2$ watersheds (Fig. 6). For example, an increase in denudation rates is seen at around 3 million years as the Neckar River and tributaries changed their drainage system from the Danube River to the Rhine River. Four pulses of incision are reported from the Laimerhöhle cave draining today into the Fils River, a tributary of the Neckar River (Strasser et al., 2009; red dots). Incision pulses 1–3 are attributed to the Danube River and indicate rates of $0.004\text{--}0.017 \text{ mm yr}^{-1}$, while pulse 4 is attributed to the Neckar River after drainage reorganization and indicates a rate of 0.700 mm yr^{-1} over 0.3 million years in the Late Pleistocene. Additionally, an increase in incision rate is reported from terraces of the Kocher River, where rates range from $0.042\text{--}0.157 \text{ mm yr}^{-1}$ before 0.78 million years, followed by rates of $0.170\text{--}0.205 \text{ mm yr}^{-1}$ at ~ 0.5 million years (Strasser et al., 2010; downward-pointing blue triangles in Fig. 6). This transient increase in rates is caused by the capture of the Ur-Kocher (original Kocher River that drained into the Danube River) by the Neckar River (Strasser et al., 2010). These transient pulses of incision are integrated, or average out, by catchment-averaged denudation rates derived from in situ-produced ^{10}Be concentrations of river sand, which integrate over millennial timescales and typically exceed decadal-timescale estimates of denudation from river load (Fig. S8).

To summarize, decadal- and millennial-timescale rates are more heterogenous and higher on the Neckar-draining side than on the Danube-draining side of the Swabian Alb. In con-

trast, million-year-scale rates on both sides are comparable and in the range of the decadal-timescale rates of the Danube Swabian Alb tributaries. The rates over space and time reflect a consistent picture with lower denudation rates from the plateau and increased denudation rates at the escarpment and its foreland due to continuous escarpment retreat and associated river captures.

5.3 Evaluation of relative strengths of chemical weathering vs. physical erosion from W/D

Calculated W/D values across the Neckar and Danube rivers are higher than 0.40, indicating that denudation is generally dominated by chemical weathering (Fig. 7a). All W/D_{corr} values for the Neckar and Danube Swabian Alb tributaries are higher than 0.40, with averages of 0.74 and 0.90, respectively. This difference is due to higher physical erosion rates in the Neckar Swabian Alb tributaries than in the Danube Swabian Alb tributaries due to escarpment retreat and river capture events (Fig. 4b). The high W/D_{corr} values, which indicate that chemical weathering is the dominant lowering process, are comparable to other German rivers, such as the Weser River (0.99) and the Elbe River (0.95), and to the Seine River (0.92) in France (Fig. 7a, Table S15a; Gaillardet et al., 1999). The high values are common for catchments in low-relief mountain ranges with mainly mixed sedimentary lithologies under temperate climatic conditions. However, they are in contrast to W/D values of almost 0 from catchments in quartz-rich lithologies (Table S15a; West et al., 2005), in more active tectonic settings (e.g., Amazon (0.19) or Brahmaputra (0.09); Gaillardet et al., 1999), or under different climatic conditions (e.g., Nile (0.27) or Niger (0.18); Gaillardet et al., 1999).

A large spread in W/D values is also reported from values based on cosmogenic nuclides for the total denudation and river load for chemical weathering rates (Fig. 7b and Table S15B). W/D values from the Apennines, a tectonically active mountain range with mixed lithologies, range from 0–1.0 (Erlanger et al., 2021). W/D values reported from tropical Cuba with mixed lithologies and tectonic uplift around $0.02\text{--}0.11\text{ mm yr}^{-1}$ (Muhs et al., 2017) range from 0.3 for igneous rocks to 0.96 for sedimentary rocks (Campbell et al., 2022). In contrast, W/D values from Panama, an active tectonic setting with igneous rocks under a tropical climate, reveal values below 0.4 (Gonzales et al., 2016). Higher W/D values than in Panama are reported for metamorphic crystalline basement rocks in tropical climates such as Sri Lanka (von Blanckenburg et al., 2004) and Cameroon (Regard et al., 2016).

Compared to other techniques that integrate over longer timescales and are more representative of landscape evolution (e.g., Riebe et al., 2003; Riebe and Granger, 2013), catchment river loads integrate chemical weathering and physical erosion across diverse bedrock lithologies and include weathering processes that occur in a deeply karstified environment (e.g., Campbell et al., 2022). However, W/D values derived from river loads can be elevated if E values derived from suspended sediment flux are underestimated relative to the total sediment fluxes that integrate longer timescales (Pratt-Sitaula et al., 2007). The Neckar and Danube drainage systems both include variations in bedrock stratigraphy and deep weathering processes, and, despite the short integration period of river load measurements, calculated denudation rates reflect long-term rates of regional rock uplift and can provide insights into the mechanics of escarpment retreat in packages of layered sedimentary rock.

Climate, tectonics, and lithology have an important influence on W and W/D values, as reported by Riebe et al. (2004). W/D values (Fig. 7c and Table S15C) were calculated based on total denudation from cosmogenic nuclides in river sediment in combination with W derived from the abundance of immobile elements in soil and rock. The method of cosmogenic nuclides in combination with immobile elements is considered to determine D and W over a similar timescale. Unfortunately, this method of in situ-produced cosmogenic ^{10}Be in river sediment is restricted to quartz-rich lithologies. The method of in situ-produced cosmogenic ^{36}Cl can be applied to carbonates for D but still relies on W from river load (e.g., Ott et al., 2019, 2023). The combination of in situ-produced cosmogenic ^{10}Be and ^{36}Cl in quartz-bearing lithologies allows the determination of D and W (Fig. 7c; Ott et al., 2024). Another promising new tool to determine D and W over similar timescales in lithologies devoid of quartz (Fig. 7d and Table S15D) is the method of meteoric ^{10}Be in river load (von Blanckenburg, et al., 2012; Wittmann et al., 2015, 2024; Dannhaus et al., 2018). Despite the increasing number of methods allowing the quantification of W , E , and D , disentangling the importance of lithology, tectonics, cli-

mate/biota, and anthropogenic impact remains challenging. Future studies (e.g., meteoric ^{10}Be) should be applied in several simple natural settings differing by only one factor.

6 Conclusions

The denudational imprint of tectonics and lithology in a region with similar climate and biota has been addressed using decadal-timescale catchment-wide physical erosion and chemical weathering rates from suspended and dissolved river load in the Swabian Alb (southwestern Germany). Our evaluation of the questions addressed in this study include the following:

- i. How do lithology and topography determine decadal-timescale W , E , and D in the context of driving escarpment retreat? The results and interpretations presented here suggest that lithologic (e.g., carbonate and sulfate bearing rocks) and base-level differences for catchments on either side of the Swabian Alb co-conspire to produce marked differences in chemical weathering and physical erosion rates.
- ii. How do these decadal-timescale rates compare to rates of landscape evolution over millennial and longer timescales? Rates over decadal-, millennial-, and million-year timescales from the Danube-draining side of the Swabian Alb report relatively homogenous surface change rates close to the uplift rate over the last 17.5 Ma. In contrast, millennial- and decadal-timescale denudation rates on the Neckar-draining side are generally up to 1 order higher than on the Danube-draining side, due to catchments recovering from stream capture and escarpment retreat of the Swabian Alb.
- iii. How do values of W/D in the Swabian Alb compare to global values of W/D ? Total denudation rates are generally dominated by chemical weathering, with W/D values as high as 0.99. While the Danube Swabian Alb tributaries are governed by chemical weathering, Neckar Swabian Alb tributaries show higher physical erosion due to escarpment retreat and river capture events. Average total denudation rates, and thus morphological activity from the Neckar Swabian Alb tributaries with their higher relief, are 2 times higher than rates from the Danube Swabian Alb tributaries. Subsequent estimated retreat rates of the Swabian Alb escarpment range from $1.0\text{--}8.1\text{ mm yr}^{-1}$. Comparable chemical weathering over total denudation rates (W/D) from catchments in different lithologic, tectonic, and climatic/biotic settings reported with river load and in situ-produced cosmogenic nuclides reveals a complex interplay of processes. To better understand rates and processes, several simple natural settings differing by only one factor should be investigated with a single method.

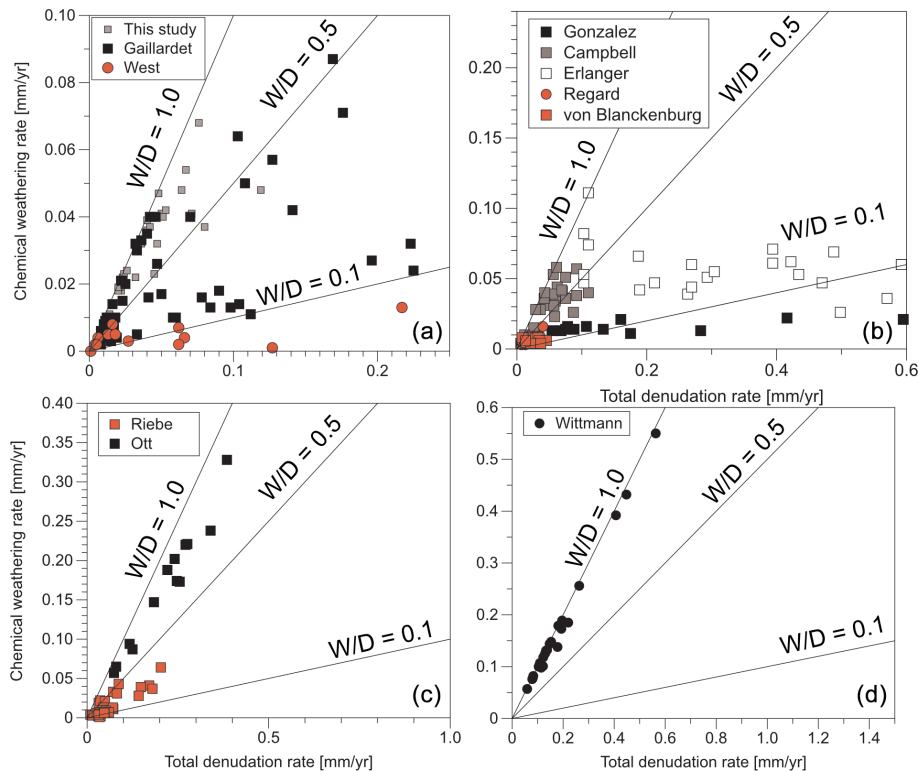


Figure 7. Comparison of chemical weathering to total denudation ratios (W/D) between this study and previous work. Chemical weathering rates versus total denudation rates with lines for W/D of 0.1, 0.5, and 1.0. Red symbols indicate data based on catchments with dominantly quartz-bearing lithologies, respectively. (a) Data based on river load (e.g., Gaillardet et al., 1999; West et al., 2005; and this study). (b) Data based on cosmogenic nuclides and river load in mixed lithologies (e.g., Gonzalez et al., 2016; Erlanger et al., 2021; Campbell et al., 2022) and quartz-rich lithologies (e.g., von Blanckenburg et al., 2004; Regard et al., 2016). (c) Data based on cosmogenic nuclides and immobile elements in quartz-rich lithologies (Riebe et al., 2003) and on paired cosmogenic nuclides in carbonate lithologies (Ott et al., 2024). (d) Data based on meteoric $^{10}\text{Be}/^9\text{Be}$ in limestone (Wittmann et al., 2024).

- iv. To what degree are anthropogenic disturbances to the catchments important for the determination of W and E ? Results indicate a strong correlation of decadal-timescale rates with different indices for anthropogenic disturbances. The magnitude of these correlations is similar to that of other “natural” factors considered (e.g., lithology, relief). Despite the significance of anthropogenic processes on rates, after correction of them, the general trend of higher rates in the Neckar rather than the Danube Swabian Alb tributaries persists, and meaningful geomorphic interpretations can be made in the region. However, future work is needed to more accurately correct W , E , and D for anthropogenic impact indices.

Code availability. The code used in this study for the calculation of retreat rates from river load denudation rates is based on Wang and Willett (2021) and available at <https://doi.org/10.5281/zenodo.15918798> (Schaller et al., 2025).

Data availability. The new data presented in this study used for calculation of chemical weathering, physical erosion, and total denudation are available at <https://doi.org/10.5281/zenodo.13588248> (Schaller et al., 2024).

Supplement. The supplement related to this article is available online at <https://doi.org/10.5194/esurf-13-571-2025-supplement>.

Author contributions. MS collected the data, wrote the text, and created the figures with DP. All co-authors wrote specific sections of the article.

Competing interests. The contact author has declared that none of the authors has any competing interests.

Disclaimer. Publisher’s note: Copernicus Publications remains neutral with regard to jurisdictional claims made in the text, published maps, institutional affiliations, or any other geographical representation in this paper. While Copernicus Publications makes ev-

ery effort to include appropriate place names, the final responsibility lies with the authors.

Acknowledgements. We would like to thank Richard Ott and Stefanie Tofelde for constructive comments improving the article.

Financial support. This research has been supported by the Bundesgesellschaft für Endlagerung (grant no. STAFuE-21-12-Klei).

Review statement. This paper was edited by Fiona Clubb and reviewed by Richard Ott and Stefanie Tofelde.

References

- Abel, T., Hinderer, M., and Sauter, M.: Karst genesis of the Swabian Alb, south Germany, since the Pliocene, *Acta Geol. Pol.*, 52, 43–54, 2002.
- Agster, G.: Ein- und Austrag sowie Umsatz gelöster Stoffe in den Einzugsgebieten des Schönbuchs, in: *Das landschaftsökologische Forschungsprojekt Naturpark Schönbuch*, VCH, Weinheim, DFG-Forschungsbericht, 343–356, 1986.
- Ahnert, F.: Functional relationships between denudation, relief, and uplift in large, mid-latitude drainage basins, *Am. J. Sci.*, 268, 243–263, <https://doi.org/10.2475/ajs.268.3.243>, 1970.
- Bauer, M.: Wasserhaushalt, aktueller und holozäner Lösungsabtrag im Wutachgebiet (Südschwarzwald), Dissertation Universität Tübingen, Tübinger Geowiss. Arbeiten (TGA), Reihe C, 14–121, 1993.
- BGR: Bundesanstalt für Geowissenschaften und Rohstoffe, Geologische Übersichtskarte der Bundesrepublik Deutschland 1 : 250000 (GÜK250, WMS), Bundesanstalt für Geowissenschaften und Rohstoffe (BGR), UUID 1780a06-69b6-44b0-855e-dc0f8da9a1d4, 2019.
- Blöthe, J. H. and Hoffmann, T.: Spatio-temporal differences dominate suspended sediment dynamics in medium-sized catchments in central Germany, *Geomorphology*, 418, 108462, <https://doi.org/10.1016/j.geomorph.2022.108462>, 2022.
- Brown, E. T., Stallard, R. F., Larsen, M. C., Raisbeck, G. M., and Yiou, F.: Denudation rates determined from the accumulation of in situ-produced ^{10}Be in the Luquillo Experimental Forest, Puerto Rico, *Earth Planet. Sc. Lett.*, 129, 193–202, [https://doi.org/10.1016/0012-821X\(94\)00249-X](https://doi.org/10.1016/0012-821X(94)00249-X), 1995.
- Bufe, A., Rugenstein, J. K. C., and Hovius, N.: CO_2 drawdown from weathering is maximized at moderate erosion rates, *Science*, 383, 1075–1080, <https://doi.org/10.1126/science.adk0957>, 2024.
- Burke, B. C., Heimsath, A. M., and White, A. F.: Coupling chemical weathering with soil production across soil-mantled landscapes, *Earth Surf. Proc. Land.*, 32, 853–873, <https://doi.org/10.1002/esp.1443>, 2007.
- Campbell, M. K., Bierman, P. R., Schmidt, A. H., Sibello Hernández, R., García-Moya, A., Corbett, L. B., Hidy, A. J., Cartas Águila, H., Guillén Arruebarrena, A., Balco, G., Dethier, D., and Caffee, M.: Cosmogenic nuclide and solute flux data from central Cuban rivers emphasize the importance of both physical and chemical mass loss from tropical landscapes, *Geochronology*, 4, 435–453, <https://doi.org/10.5194/gchron-4-435-2022>, 2022.
- Cole, J. J. and Prairie, Y. T.: Dissolved CO_2 in Freshwater Systems, Reference Module in Earth Systems and Environmental Sciences, 30–34, <https://doi.org/10.1016/B978-0-12-409548-9.09399-4>, 2014.
- Dannhaus, N., Wittmann, H., Krám, P., Christl, M., and von Blanckenburg, F.: Catchment-wide weathering and erosion rates of mafic, ultramafic, and granitic rock from cosmogenic meteoric $^{10}\text{Be}/^9\text{Be}$ ratios, *Geochim. Cosmochim. Ac.*, 222, 618–641, <https://doi.org/10.1016/j.gca.2017.11.005>, 2018.
- Davis, W. M.: The Drainage of Cuestas, *P. Geologists Assoc.*, 16, 75–93, [https://doi.org/10.1016/S0016-7878\(99\)80031-5](https://doi.org/10.1016/S0016-7878(99)80031-5), 1899.
- Dethier, E. N., Renshaw, C. E., and Magilligan, F. J.: Rapid changes to global river suspended sediment flux by humans, *Science*, 376, 1447–1452, <https://doi.org/10.1126/science.abn7980>, 2022.
- DGJ: Deutsches Gewässerkundliches Jahrbuch Rheingebiet, Teil I, 2009, Landesanstalt für Umweltschutz Baden-Württemberg, 2012.
- DGJ: Deutsches Gewässerkundliches Jahrbuch Donaugebiet 2006, Bayerisches Landesamt für Umwelt, ISSN 2190-9954, 2014.
- DiBiase, R. A., Whipple, K. X., Heimsath, A. M., and Ouimet, W. B.: Landscape form and millennial erosion rates in the San Gabriel Mountains, CA, *Earth Planet. Sc. Lett.*, 289, 134–144, <https://doi.org/10.1016/j.epsl.2009.10.036>, 2010.
- Dietrich, W. E. and Perron, J. T.: The search for a topographic signature of life, *Nature*, 439, 411–418, <https://doi.org/10.1038/nature04452>, 2006.
- Dixon, J. L., Heimsath, A. M., and Amundson, R.: The critical role of climate and saprolite weathering in landscape evolution, *Earth Surf. Proc. Land.*, 34, 1507–1521, <https://doi.org/10.1002/esp.1836>, 2009.
- Dongus, H.: Die Oberflächenformen der Schwäbischen Alb und ihres Vorlands, vol. 72, Marburger geographische Schriften, 460–486, ISSN 0341-9290, 2000.
- Duszyński, F., Migoń, P., and Strzelecki, M. C.: Escarpment retreat in sedimentary tablelands and cuesta landscapes – Landforms, mechanisms and patterns, *Earth-Sci. Rev.*, 196, 102890, <https://doi.org/10.1016/j.earscirev.2019.102890>, 2019.
- Ehlers, T. A., Chen, D., Appel, E., Bolch, T., Chen, F., Diekmann, B., Dippold, M. A., Giese, M., Guggenberger, G., Lai, H.-W., Li, X., Liu, J., Liu, Y., Ma, Y., Miede, G., Mosbrugger, V., Mulch, A., Piao, S., Schwalb, A., Thompson, L. G., Su, Z., Sun, H., Yao, T., Yang, X., Yang, K., and Zhu, L.: Past, present, and future geo-biosphere interactions on the Tibetan Plateau and implications for permafrost, *Earth-Sci. Rev.*, 234, 104197, <https://doi.org/10.1016/j.earscirev.2022.104197>, 2022.
- Erlanger, E. D., Rugenstein, J. K. C., Bufe, A., Picotti, V., and Willett, S. D.: Controls on Physical and Chemical Denudation in a Mixed Carbonate-Siliciclastic Orogen, *J. Geophys. Res.-Earth*, 126, e2021JF006064, <https://doi.org/10.1029/2021JF006064>, 2021.
- European Commission Directorate – General Joint Research Centre: Normalised Difference Vegetation Index Statistics 1999–2019 (raster 1 km), global, 10-daily, version 3, https://land.copernicus.vgt.vito.be/geonetwork/srv/api/records/urn:cgl:global:ndvi_stats_all (last access: 10 December 2024), 2021.

- Flint, J. J.: Stream gradient as a function of order, magnitude, and discharge, *Water Resour. Res.*, 10, 969–973, <https://doi.org/10.1029/WR010i005p00969>, 1974.
- Forté, A. M. and Whipple, K. X.: Short communication: The Topographic Analysis Kit (TAK) for TopoToolbox, *Earth Surf. Dynam.*, 7, 87–95, <https://doi.org/10.5194/esurf-7-87-2019>, 2019.
- Gaillardet, J., Dupré, B., Louvat, P., and Allègre, C. J.: Global silicate weathering and CO₂ consumption rates deduced from the chemistry of large rivers, *Chem. Geol.*, 159, 3–30, [https://doi.org/10.1016/S0009-2541\(99\)00031-5](https://doi.org/10.1016/S0009-2541(99)00031-5), 1999.
- GKD: Gewässerkundlicher Dienst Bayern, <https://www.gkd.bayern.de/>, last access: 15 January 2023.
- Granger, D. E., Kirchner, J. W., and Finkel, R.: Spatially Averaged Long-Term Erosion Rates Measured from in Situ-Produced Cosmogenic Nuclides in Alluvial Sediment, *J. Geol.*, 104, 249–257, <https://doi.org/10.1086/629823>, 1996.
- Grill, G., Lehner, B., Thieme, M., Geenen, B., Tickner, D., Antonelli, F., Babu, S., Borrelli, P., Cheng, L., Crochetiere, H., Ehalt Macedo, H., Filgueiras, R., Goichot, M., Higgins, J., Hogan, Z., Lip, B., McClain, M. E., Meng, J., Mulligan, M., Nilsson, C., Olden, J. D., Opperman, J. J., Petry, P., Reidy Liermann, C., Sáenz, L., Salinas-Rodríguez, S., Schelle, P., Schmitt, R. J. P., Snider, J., Tan, F., Tockner, K., Valdujo, P. H., Van Soesbergen, A., and Zarfl, C.: Mapping the world's free-flowing rivers, *Nature*, 569, 215–221, <https://doi.org/10.1038/s41586-019-1111-9>, 2019.
- Harel, M.-A., Mudd, S. M., and Attal, M.: Global analysis of the stream power law parameters based on worldwide 10 Be denudation rates, *Geomorphology*, 268, 184–196, <https://doi.org/10.1016/j.geomorph.2016.05.035>, 2016.
- He, C., Braun, J., Tang, H., Yuan, X., Acevedo-Trejos, E., Ott, R. F., and Stucky De Quay, G.: Drainage divide migration and implications for climate and biodiversity, *Nat. Rev. Earth Environ.*, 5, 177–192, <https://doi.org/10.1038/s43017-023-00511-z>, 2024.
- Heimsath, A. M. and Burke, B.: The impact of local geochemical variability on quantifying hillslope soil production and chemical weathering, *Geomorphology*, 200, 75–88, 2013.
- Hewawasam, T., von Blanckenburg, F., Schaller, M., and Kubik, P.: Increase of human over natural erosion rates in tropical highlands constrained by cosmogenic nuclides, *Geology*, 31, 597–600, [https://doi.org/10.1130/0091-7613\(2003\)031<0597:IOHONE>2.0.CO;2](https://doi.org/10.1130/0091-7613(2003)031<0597:IOHONE>2.0.CO;2), 2003.
- Hinderer, M.: Stoffbilanzen in kleinen Einzugsgebieten Baden-Württembergs: Herrn Professor Gerhard Einsele zum 80. Geburtstag gewidmet, *Grundwasser*, 11, 164–178, <https://doi.org/10.1007/s00767-006-0142-y>, 2006.
- Hoffmann, M.: Young tectonic evolution of the Northern Alpine Foreland Basin, southern Germany, based on linking geomorphology and structural geology, Dissertation, Ludwig Maximilian University of Munich 212 pp., <https://doi.org/10.5282/edoc.21123>, 2017.
- Hoffmann, T. O., Baulig, Y., Vollmer, S., Blöthe, J. H., Auerwald, K., and Fiener, P.: Pristine levels of suspended sediment in large German river channels during the Anthropocene?, *Earth Surf. Dynam.*, 11, 287–303, <https://doi.org/10.5194/esurf-11-287-2023>, 2023.
- Hofmann, F., Reichenbacher, B., and Farley, K. A.: Evidence for > 5 Ma paleo-exposure of an Eocene–Miocene paleosol of the Bohnerz Formation, Switzerland, *Earth Planet. Sc. Lett.*, 465, 168–175, <https://doi.org/10.1016/j.epsl.2017.02.042>, 2017.
- Holzwarth, W.: Wasserhaushalt und Stoffumsatz kleiner Einzugsgebiete im Keuper und Jura bei Reutlingen – Tübingen, Tübingen, 1980.
- Hönle, J.: Karstdenudation auf dem Gebiet der Schwabischen Alb, *Mitt. Verb. dt. Höhlen- u. Karstforsch.*, 37, 480–52, 1991.
- Karger, D. N., Conrad, O., Böhner, J., Kawohl, T., Kreft, H., Soria-Auza, R. W., Zimmermann, N. E., Linder, H. P., and Kessler, M.: Climatologies at high resolution for the earth's land surface areas, *Scientific Data*, 4, sdata2017122, <https://doi.org/10.1038/sdata.2017.122>, 2017.
- Karger, D. N., Conrad, O., Böhner, J., Kawohl, T., Kreft, H., Soria-Auza, R. W., Zimmermann, N. E., Linder, H. P., and Kessler, M.: Climatologies at high resolution for the earth's land surface areas CHELSA V2.1 [data set] (current) (2.1), <https://doi.org/10.16904/ENVIDAT.228.V2.1>, 2021.
- Katz, B. G., Bricker, O. P., and Kennedy, M. M.: Geochemical mass-balance relationships for selected ions in precipitation and stream water, Catoctin Mountains, Maryland, *Am. J. Sci.*, 285, 931–962, 1985.
- Kirby, E. and Whipple, K. X.: Expression of active tectonics in erosional landscapes, *J. Struct. Geol.*, 44, 54–75, <https://doi.org/10.1016/j.jsg.2012.07.009>, 2012.
- Larsen, I. J., Almond, P. C., Eger, A., Stone, J. O., Montgomery, D. R., and Malcolm, B.: Rapid Soil Production and Weathering in the Southern Alps, New Zealand, *Science*, 343, 637–640, <https://doi.org/10.1126/science.1244908>, 2014.
- Landesamt für Geoinformation und Landentwicklung Baden-Württemberg (LGL-BW): ATKIS Digitales Geländemodell DGM 5 m, GDI-DE Registry, <https://registry.gdi-de.org/id/de.bw.lubw.mdk/dc988bd8-2bbb-4e88-91fc-1daf196eeef6> (last access: 10 July 2025), 2005.
- León-Tavares, J., Roujean, J.-L., Smets, B., Wolters, E., Toté, C., and Swinnen, E.: Correction of Directional Effects in VEGETATION NDVI Time-Series, *Remote Sens.*, 13, 1130, <https://doi.org/10.3390/rs13061130>, 2021.
- Littke, R., Bayer, U., Gajewski, D., and Nelskamp, S.: Dynamics of complex intracontinental basins: the Central European Basin System, Springer, Berlin, ISBN 978-3-540-85084-7, 2008.
- LUBW: Karten und Datendienst der LUBW: <https://udo.lubw.baden-wuerttemberg.de/public/>, last access: 15 January 2023.
- Maher, K. and Chamberlain, C. P.: Hydrologic Regulation of Chemical Weathering and the Geologic Carbon Cycle, *Science*, 343, 1502–1504, <https://doi.org/10.1126/science.1250770>, 2014.
- Malinowski, R., Lewiński, S., Rybicki, M., Gromny, E., Jenerowicz, M., Krupiński, M., Nowakowski, A., Wojtkowski, C., Krupiński, M., Krätzschmar, E., and Schauer, P.: Automated Production of a Land Cover/Use Map of Europe Based on Sentinel-2 Imagery, *Remote Sens.*, 12, 3523, <https://doi.org/10.3390/rs12213523>, 2020.
- Meybeck, M.: Composition chimique des ruisseaux non pollués en France, Chemical composition of headwater streams in France, *sgeol*, 39, 3–77, <https://doi.org/10.3406/sgeol.1986.1719>, 1986.
- Montgomery, D. R. and Brandon, M. T.: Topographic controls on erosion rates in tectonically active mountain ranges, *Earth Planet. Sc. Lett.*, 201, 481–489, [https://doi.org/10.1016/S0012-821X\(02\)00725-2](https://doi.org/10.1016/S0012-821X(02)00725-2), 2002.

- Morel, P., von Blanckenburg, F., Schaller, M., Kubik, P. W., and Hinderer, M.: Lithology, landscape dissection and glaciation controls on catchment erosion as determined by cosmogenic nuclides in river sediment (the Wutach Gorge, Black Forest), *Terra Nova*, 15, 398–404, <https://doi.org/10.1046/j.1365-3121.2003.00519.x>, 2003.
- Mu, H., Li, X., Wen, Y., Huang, J., Du, P., Su, W., Miao, S., and Geng, M.: A global record of annual terrestrial Human Footprint dataset from 2000 to 2018, *Scientific Data*, 9, 176, <https://doi.org/10.1038/s41597-022-01284-8>, 2022.
- Muhs, D. R., Schweig, E. S., Simmons, K. R., and Halley, R. B.: Late Quaternary uplift along the North America-Caribbean plate boundary: Evidence from the sea level record of Guantanamo Bay, Cuba, *Quaternary Sci. Rev.*, 178, 54–76, <https://doi.org/10.1016/j.quascirev.2017.10.024>, 2017.
- Ott, R. F., Gallen, S. F., Caves Rugenstein, J. K., Ivy-Ochs, S., Helman, D., Fassoulas, C., Vockenhuber, C., Christl, M., and Willett, S. D.: Chemical Versus Mechanical Denudation in Meta-Clastic and Carbonate Bedrock Catchments on Crete, Greece, and Mechanisms for Steep and High Carbonate Topography, *J. Geophys. Res.-Earth*, 124, 2943–2961, <https://doi.org/10.1029/2019JF005142>, 2019.
- Ott, R. F., Gallen, S. F., and Granger, D. E.: Cosmogenic nuclide weathering biases: corrections and potential for denudation and weathering rate measurements, *Geochronology*, 4, 455–470, <https://doi.org/10.5194/gchron-4-455-2022>, 2022.
- Ott, R. F., Gallen, S. F., and Helman, D.: Erosion and weathering in carbonate regions reveal climatic and tectonic drivers of carbonate landscape evolution, *EGU sphere* [preprint], <https://doi.org/10.5194/egusphere-2022-1376>, 2023.
- Ott, R. F., Kober, F., Ivy-Ochs, S., Scherler, D., von Blanckenburg, F., Christl, M., and Vockenhuber, C.: Erosion-weathering partitioning from paired-mineral and weathering-corrected cosmogenic nuclide approaches, *Quaternary Sci. Rev.*, 348, 109114, <https://doi.org/10.1016/j.quascirev.2024.109114>, 2024.
- Peifer, D., Persano, C., Hurst, M. D., Bishop, P., and Fabel, D.: Growing topography due to contrasting rock types in a tectonically dead landscape, *Earth Surf. Dynam.*, 9, 167–181, <https://doi.org/10.5194/esurf-9-167-2021>, 2021.
- Pelletier, J. D., Broxton, P. D., Hazenberg, P., Zeng, X., Troch, P. A., Niu, G., Williams, Z., Brunke, M. A., and Gochis, D.: A gridded global data set of soil, intact regolith, and sedimentary deposit thicknesses for regional and global land surface modeling, *J. Adv. Model. Earth Syst.*, 8, 41–65, <https://doi.org/10.1002/2015MS000526>, 2016.
- Petit, C., Campy, M., Chaline, J., and Bonvalot, J.: Major palaeohydrographic changes in Alpine foreland during the Pliocene - Pleistocene, *Boreas*, 25, 131–143, <https://doi.org/10.1111/j.1502-3885.1996.tb00841.x>, 1996.
- Poppe, R.: Eintiefungsgeschichte und Stoffausttrag im Wutachgebiet (SW-Deutschland), in: Karstsystem und Lösungsausttrag im oberen Jura des Aitrachtals, in: Eintiefungsgeschichte und Stoffausttrag im Wutachgebiet (SW-Deutschland), edited by: Einsele, G. and Ricken, W., Tübingen, Tübinger Geowiss. Arbeiten (TGA), 181–188, 1993.
- Portenga, E. W. and Bierman, P. R.: Understanding Earth's eroding surface with ^{10}Be , *GSA Today*, 21, 4–10, <https://doi.org/10.1130/G111A.1>, 2011.
- Pratt-Sitaula, B., Garde, M., Burbank, D. W., Oskin, M., Heimsath, A., and Gabet, E.: Bedload-to-suspended load ratio and rapid bedrock incision from Himalayan Landslide-dam lake record, *Quaternary Res.*, 68, 111–120, <https://doi.org/10.1016/j.yqres.2007.03.005>, 2007.
- Raymo, M. E., Ruddiman, W. F., and Froelich, P. N.: Influence of late Cenozoic mountain building on ocean geochemical cycles, *Geol.*, 16, 649, [https://doi.org/10.1130/0091-7613\(1988\)016<0649:IOLCMB>2.3.CO;2](https://doi.org/10.1130/0091-7613(1988)016<0649:IOLCMB>2.3.CO;2), 1988.
- Regard, V., Carretier, S., Boeglin, J., Ndam Ngoupayou, J., Dzana, J., Bedimo Bedimo, J., Riotte, J., and Braun, J.: Denudation rates on cratonic landscapes: comparison between suspended and dissolved fluxes, and ^{10}Be analysis in the Nyong and Sanaga River basins, south Cameroon, *Earth Surf. Proc. Land.*, 41, 1671–1683, <https://doi.org/10.1002/esp.3939>, 2016.
- Riebe, C. S. and Granger, D. E.: Quantifying effects of deep and near-surface chemical erosion on cosmogenic nuclides in soils, saprolite, and sediment: Effects of chemical erosion on cosmogenic nuclide buildup, *Earth Surf. Proc. Land.*, 38, 523–533, <https://doi.org/10.1002/esp.3339>, 2013.
- Riebe, C. S., Kirchner, J. W., and Finkel, R. C.: Long-term rates of chemical weathering and physical erosion from cosmogenic nuclides and geochemical mass balance, *Geochim. Cosmochim. Ac.*, 67, 4411–4427, [https://doi.org/10.1016/S0016-7037\(03\)00382-X](https://doi.org/10.1016/S0016-7037(03)00382-X), 2003.
- Riebe, C. S., Kirchner, J. W., and Finkel, R. C.: Erosional and climatic effects on long-term chemical weathering rates in granitic landscapes spanning diverse climate regimes, *Earth Planet. Sc. Lett.*, 224, 547–562, <https://doi.org/10.1016/j.epsl.2004.05.019>, 2004.
- Ring, U. and Bolhar, R.: Tilting, uplift, volcanism and disintegration of the South German block, *Tectonophysics*, 795, 228611, <https://doi.org/10.1016/j.tecto.2020.228611>, 2020.
- Ross, M. R. V., Nippgen, F., Hassett, B. A., McGlynn, B. L., and Bernhardt, E. S.: Pyrite Oxidation Drives Exceptionally High Weathering Rates and Geologic CO_2 Release in Mountaintop-Mined Landscapes, *Global Biogeochem. Cy.*, 32, 1182–1194, <https://doi.org/10.1029/2017GB005798>, 2018.
- Ryb, U., Matmon, A., Erel, Y., Haviv, I., Benedetti, L., and Hidy, A. J.: Styles and rates of long-term denudation in carbonate terrains under a Mediterranean to hyper-arid climatic gradient, *Earth Planet. Sc. Lett.*, 406, 142–152, <https://doi.org/10.1016/j.epsl.2014.09.008>, 2014.
- Schaller, M. and Ehlers, T. A.: Comparison of soil production, chemical weathering, and physical erosion rates along a climate and ecological gradient (Chile) to global observations, *Earth Surf. Dynam.*, 10, 131–150, <https://doi.org/10.5194/esurf-10-131-2022>, 2022.
- Schaller, M., von Blanckenburg, F., Hovius, N., and Kubik, P. W.: Large-scale erosion rates from in situ-produced cosmogenic nuclides in European river sediments, *Earth Planet. Sc. Lett.*, 188, 441–458, [https://doi.org/10.1016/S0012-821X\(01\)00320-X](https://doi.org/10.1016/S0012-821X(01)00320-X), 2001.
- Schaller, M., von Blanckenburg, F., Veldkamp, A., Tebbens, L. A., Hovius, N., and Kubik, P. W.: A 30 000 yr record of erosion rates from cosmogenic ^{10}Be in Middle European river terraces, *Earth Planet. Sc. Lett.*, 204, 307–320, [https://doi.org/10.1016/S0012-821X\(02\)00951-2](https://doi.org/10.1016/S0012-821X(02)00951-2), 2002.

- Schaller, M., Peifer, D., Neely, A. B., Bernard, T., Glotzbach, C., Beer, A. R., and Ehlers, T. A.: Spatiotemporal denudation rates of the Swabian Alb escarpment (Southwest Germany) dominated by anthropogenic impact, lithology, and base-level lowering, Zenodo [data set], <https://doi.org/10.5281/zenodo.13588248>, 2024.
- Schaller, M., Peifer, D., Neely, A. B., Bernard, T., Glotzbach, C., Beer, A. R., and Ehlers, T. A.: Spatiotemporal denudation rates of the Swabian Alb escarpment (Southwest Germany) dominated by anthropogenic impact, lithology, and base-level lowering, Zenodo [code], <https://doi.org/10.5281/zenodo.15918798>, 2025.
- Schwanghart, W. and Scherler, D.: Short Communication: Topo-Toolbox 2 – MATLAB-based software for topographic analysis and modeling in Earth surface sciences, *Earth Surf. Dynam.*, 2, 1–7, <https://doi.org/10.5194/esurf-2-1-2014>, 2014.
- Sharma, H. and Ehlers, T. A.: Effects of seasonal variations in vegetation and precipitation on catchment erosion rates along a climate and ecological gradient: insights from numerical modeling, *Earth Surf. Dynam.*, 11, 1161–1181, <https://doi.org/10.5194/esurf-11-1161-2023>, 2023.
- Sosa Gonzalez, V., Bierman, P. R., Fernandes, N. F., and Rood, D. H.: Long-term background denudation rates of southern and southeastern Brazilian watersheds estimated with cosmogenic ^{10}Be , *Geomorphology*, 268, 54–63, <https://doi.org/10.1016/j.geomorph.2016.05.024>, 2016.
- Strasser, A., Strasser, M., and Seyfried, H.: Quantifying erosion over timescales of one million years: A photogrammetric approach on the amount of Rhenish erosion in southwestern Germany, *Geomorphology*, 122, 244–253, <https://doi.org/10.1016/j.geomorph.2009.06.027>, 2010.
- Strasser, M., Strasser, A., Pelz, K., and Seyfried, H.: A mid Miocene to early Pleistocene multi-level cave as a gauge for tectonic uplift of the Swabian Alb (Southwest Germany), *Geomorphology*, 106, 130–141, <https://doi.org/10.1016/j.geomorph.2008.09.012>, 2009.
- Terhorst, B.: Mass movements of various ages on the Swabian Jurassic escarpment: geomorphologic processes and their causes, *Z. Geomorphol. N. F.*, 125, 65–87, 2001.
- Thiebes, B.: Landslide analysis and early warning Local and regional case study in the Swabian Alb, Germany, Wien, 279 pp., 2011.
- Thury, M.: The characteristics of the Opalinus Clay investigated in the Mont Terri underground rock laboratory in Switzerland, *C. R. Phys.*, 3, 923–933, [https://doi.org/10.1016/S1631-0705\(02\)01372-5](https://doi.org/10.1016/S1631-0705(02)01372-5), 2002.
- Turowski, J. M., Rickenmann, D., and Dadson, S. J.: The partitioning of the total sediment load of a river into suspended load and bedload: a review of empirical data: The partitioning of sediment load, *Sedimentology*, 57, 1126–1146, <https://doi.org/10.1111/j.1365-3091.2009.01140.x>, 2010.
- Ufrecht, W.: Evaluating landscape development and karstification of the Central Schwabische Alb (Southwest Germany) by fossil record of karst fillings, *zfg*, 52, 417–436, <https://doi.org/10.1127/0372-8854/2008/0052-0417>, 2008.
- Ufrecht, W.: Abfolge und Alter der Neckar-Terrassen und Travertine in Stuttgart (Cannstatter Becken und Nesenbachtal), *Jahreshefte der Gesellschaft für Naturkunde in Württemberg*, 178, 253–324, <https://doi.org/10.26251/JHGFN.178.2022.253-324>, 2022.
- Ufrecht, W., Bohnert, J., and Jantschke, H.: Ein konzeptionelles Modell der Verkarstungsgeschichte für das Einzugsgebiet des Blautopfs (mittlere Schwäbische Alb), *Laichinger Höhlenfreund*, 51, 3–44, 2016.
- Vanacker, V., von Blanckenburg, F., Govers, G., Molina, A., Poesen, J., Deckers, J., and Kubik, P.: Restoring dense vegetation can slow mountain erosion to near natural benchmark levels, *Geology*, 35, 303–306, <https://doi.org/10.1130/G23109A.1>, 2007.
- VanLandingham, L. A., Portenga, E. W., Lefroy, E. C., Schmidt, A. H., Bierman, P. R., and Hidy, A. J.: Comparison of basin-scale in situ and meteoric ^{10}Be erosion and denudation rates in felsic lithologies across an elevation gradient at the George River, northeast Tasmania, Australia, *Geochronology*, 4, 153–176, <https://doi.org/10.5194/gchron-4-153-2022>, 2022.
- Vanmaercke, M., Poesen, J., Govers, G., and Verstraeten, G.: Quantifying human impacts on catchment sediment yield: A continental approach, *Global Planet. Change*, 130, 22–36, <https://doi.org/10.1016/j.gloplacha.2015.04.001>, 2015.
- Villinger, E.: Zur Flußgeschichte von Rhein und Donau in Südwestdeutschland, *jber_oberrh.*, 80, 361–398, <https://doi.org/10.1127/jmogv/80/1998/361>, 1998.
- von Blanckenburg, F., Hewawasam, T., and Kubik, P. W.: Cosmogenic nuclide evidence for low weathering and denudation in the wet, tropical highlands of Sri Lanka, *J. Geophys. Res.*, 109, F03008, <https://doi.org/10.1029/2003JF000049>, 2004.
- von Blanckenburg, F., Bouchez, J., and Wittmann, H.: Earth surface erosion and weathering from the ^{10}Be (meteoric)/ ^9Be ratio, *Earth Planet. Sc. Lett.*, 351–352, 295–305, <https://doi.org/10.1016/j.epsl.2012.07.022>, 2012.
- Wang, Y. and Willett, S. D.: Escarpment retreat rates derived from detrital cosmogenic nuclide concentrations, *Earth Surf. Dynam.*, 9, 1301–1322, <https://doi.org/10.5194/esurf-9-1301-2021>, 2021.
- Wang, Y., Willett, S. D., Wu, D., Haghipour, N., and Christl, M.: Retreat of the Great Escarpment of Madagascar From Geomorphic Analysis and Cosmogenic ^{10}Be Concentrations, *Geochem. Geophys. Geosy.*, 22, e2021GC009979, <https://doi.org/10.1029/2021GC009979>, 2021.
- West, A., Galy, A., and Bickle, M.: Tectonic and climatic controls on silicate weathering, *Earth Planet. Sc. Lett.*, 235, 211–228, <https://doi.org/10.1016/j.epsl.2005.03.020>, 2005.
- Winterberg, S. and Willett, S. D.: Greater Alpine river network evolution, interpretations based on novel drainage analysis, *Swiss J. Geosci.*, 112, 3–22, <https://doi.org/10.1007/s00015-018-0332-5>, 2019.
- Wittmann, H., von Blanckenburg, F., Dannhaus, N., Bouchez, J., Gaillardet, J., Guyot, J. L., Maurice, L., Roig, H., Filizola, N., and Christl, M.: A test of the cosmogenic ^{10}Be (meteoric)/ ^9Be proxy for simultaneously determining basin-wide erosion rates, denudation rates, and the degree of weathering in the Amazon basin: Erosion from meteoric $^{10}\text{Be}/^9\text{Be}$ in amazon, *J. Geophys. Res.-Earth*, 120, 2498–2528, <https://doi.org/10.1002/2015JF003581>, 2015.
- Wittmann, H., Bouchez, J., Calmels, D., Gaillardet, J., Frick, D., Stroncik, N., ASTER Team, and von Blanckenburg, F.: Denudation and weathering rates of carbonate landscapes from meteoric $^{10}\text{Be}/^9\text{Be}$ ratios, *GFZ Data Services*, <https://doi.org/10.5880/GFZ.3.3.2024.001>, 2024.

- Yanites, B. J., Ehlers, T. A., Becker, J. K., Schnellmann, M., and Heuberger, S.: High magnitude and rapid incision from river capture: Rhine River, Switzerland: Erosion from river capture: Rhine river, *J. Geophys. Res.-Earth*, 118, 1060–1084, <https://doi.org/10.1002/jgrf.20056>, 2013.
- Zeng, S., Liu, Z., and Kaufmann, G.: Sensitivity of the global carbonate weathering carbon-sink flux to climate and land-use changes, *Nat. Commun.*, 10, 5749, <https://doi.org/10.1038/s41467-019-13772-4>, 2019.
- Ziegler, P. A. and Fraefel, M.: Response of drainage systems to Neogene evolution of the Jura fold-thrust belt and Upper Rhine Graben, *Swiss J. Geosci.*, 102, 57–75, <https://doi.org/10.1007/s00015-009-1306-4>, 2009.